

# Dust properties of UV bright galaxies at $z \sim 2^*$

S. Noll and D. Pierini

Max-Planck-Institut für extraterrestrische Physik, Giessenbachstr., 85748 Garching, Germany  
e-mail: snoll@mpe.mpg.de

Received 14 June 2005 / Accepted 13 August 2005

## ABSTRACT

We investigate the properties of the extinction curve in the rest-frame UV for a sample of 34 UV-luminous galaxies at  $2 < z < 2.5$ , selected from the FORS Deep Field (FDF) spectroscopic survey. A new parametric description of the rest-frame UV spectral energy distribution is adopted; its sensitivity to properties of the stellar populations or of dust attenuation is established with the use of models. The latter are computed by combining composite stellar population models and calculations of radiative transfer of the stellar and scattered radiation through the dusty interstellar medium (ISM) for a dust/stars configuration describing dust attenuation in local starbursts. In the favoured configuration the stars are enveloped by a shell with a two-phase, clumpy, dusty ISM. The distribution of the  $z \sim 2$  UV-luminous FDF galaxies in several diagnostic diagrams shows that their extinction curves range between those typical of the Small and Large Magellanic Clouds (SMC and LMC, respectively). For the majority of strongly reddened objects having a UV continuum slope  $\beta > -0.4$  a significant 2175 Å absorption feature (or “UV bump”) is inferred, indicating an LMC-like extinction curve. On the other hand, the UV continua of the least reddened objects are mostly consistent with SMC-like extinction curves, lacking a significant UV bump, as for the sample of local starbursts investigated by Calzetti and collaborators. Furthermore, the most opaque ( $\beta \sim 0$ ) and, thus (for our models), dustiest UV-luminous FDF galaxies tend to be among the most metal-rich, most massive, and largest systems at  $z \sim 2$ , indicating  $\langle Z \rangle \sim 0.5\text{--}1 Z_\odot$ ,  $\langle M_{\text{stars}} \rangle \sim 6 \times 10^{10} M_\odot$ , and  $\langle R_{\text{eff}} \rangle \sim 4$  kpc, respectively. The presence of the UV bump does not seem to depend on the total metallicity, as given by the equivalent width (EW) of the C IV doublet. Conversely, it seems to be associated with a large average EW of the six most prominent interstellar low-ionisation absorption lines falling in the FORS spectra. The average EW of these saturated lines offers a proxy for the ISM topology. We interpret these results as the evidence for a difference in the properties of the dusty ISM among the most evolved UV-luminous, massive galaxies at  $z \sim 2$ .

**Key words.** galaxies: high-redshift – galaxies: starburst – galaxies: ISM – ISM: dust, extinction – ultraviolet: galaxies

## 1. Introduction

The electromagnetic radiation propagating through a medium containing dust particles experiences extinction. In general, the intensity of the transmitted beam is reduced by two physical processes: absorption and scattering. Dust grains absorb and scatter more the shorter the wavelength. As a consequence, both the total intensity and the spectrum of the pristine radiation are modified. The so-called *extinction curve* quantifies the amount of extinction as a function of wavelength along the line of sight. It depends on the chemical composition, structure, and size distribution of the intervening dust grains (Mathis et al. 1977; Désert et al. 1990; Dweck et al. 1997; Draine & Li 2001; Li & Draine 2001; Zubko et al. 2004). Hence, studies of extinction provide information on the properties of dust.

The *direct* determination of the spectral dependence of extinction from observational data is limited to our own Galaxy,

the Magellanic Clouds, and M 31 (for reviews see Fitzpatrick 2004; and Clayton 2004).

Extinction curves of our own Galaxy vary for different sight lines and towards different environments (from dense molecular clouds to the diffuse interstellar medium, ISM; see Fitzpatrick 2004). However, the extinction curves determined for the diffuse ISM of the Milky Way (MW) seem to represent a one-parameter family, the parameter being the total-to-selective extinction ratio  $R_V = A_V/E_{B-V}$  (Cardelli et al. 1989, CCM; Fitzpatrick 1999; Clayton et al. 2000; Valencic et al. 2004; see however Fitzpatrick 2004). Broadly speaking,  $R_V$  is a proxy for the average grain size: low- $R_V$  sight lines have more small grains than high- $R_V$  sight lines. The smaller the grains, the steeper the extinction curve in the ultraviolet (UV).

The average extinction curve for the diffuse ISM of the MW has  $R_V = 3.1$ . It is characterised by the presence of a bump at a constant central wavelength of 2175 Å. This absorption feature (Witt & Lillie 1973) is most likely produced by graphitic carbon, though its origin is still under discussion (Draine 2003; Whittet 2003 and references therein). The width of the UV bump seems to depend on the environment: narrow

\* Based on observations obtained with FORS at the VLT, Paranal, Chile on the course of the observing proposals 63.O-0005, 64.O-0149, 64.O-0158, 65.O-0049, 66.A-0547, 68.A-0013, 68.A-0014, 69.A-0104.

bumps tend to be associated with diffuse regions, while broad bumps favour dense regions (Valencic et al. 2004). The occurrence of weak bumps may reflect processing that modifies or destroys the bump carrier in dark clouds (Whittet et al. 2004).

The few sight lines studied in M 31 seem to show a CCM far-UV extinction and a weak 2175 Å bump (Bianchi et al. 1996). There are remarkable differences in dust grain properties between the Milky Way and the Large and Small Magellanic Clouds (LMC and SMC, respectively). The sight lines toward the LMC 2 supershell and the average LMC extinction curve exhibit a weaker bump and stronger far-UV extinction than the average MW  $R_V = 3.1$  extinction curve. The sight lines toward the SMC bar exhibit an extremely weak or absent UV bump and a very strong far-UV extinction, which is indicative of a very large fraction of small dust particles (Rodrigues et al. 1997). These differences may reflect differences in metallicity<sup>1</sup> and gas-to-dust ratio (Bohlin et al. 1978; Luck & Lambert 1992; Gordon et al. 2003).

Different environments, such as star-formation regions where large amounts of UV radiation and shocks are present, may play a fundamental role in processing dust. This is not easy to establish however. As remarked by Clayton (2004), the LMC 2 supershell is located in the 30 Dor region, which is a much larger star-forming region than any in the SMC, but the LMC 2 supershell extinction curve is in much better agreement with a CCM MW extinction curve than the SMC extinction curve. Nevertheless, it is intriguing that nearby starburst galaxies spanning a large range in metallicity (from sub- to super-solar) possibly contain dust with an extinction curve lacking a 2175 Å bump, like the SMC curve, and a steep far-UV rise, intermediate between the MW and SMC curves (Calzetti et al. 1994, 2000; Gordon et al. 1997; Leitherer et al. 2002). For these objects, the properties of dust (i.e. the extinction curve) can be determined only in an *indirect* and rough way, after resorting to models of radiative transfer of the stellar and scattered radiation through a dusty ISM (Witt & Gordon 2000, WG00; Misselt et al. 2001; Fischera et al. 2003; Inoue 2005). In fact, on a galaxy scale, the propagation of electromagnetic radiation through a dusty medium is described by the *attenuation function*, i.e. the combination of the extinction curve with the geometry of the system, in which a substantial fraction of the scattered light is returned to the observer's line of sight.

SMC-like dust seems to characterise also starburst galaxies in the distant universe. This holds for individual objects with a well-sampled SED (e.g. Gordon et al. 1999) as well as for large photometric samples, like that of  $\sim 1000$  Lyman-break galaxies (LBGs) at  $z \sim 3$  observed by Steidel et al. (2003) (Vijh et al. 2003). The absence of a 2175 Å bump seems to characterise the rest-frame UV spectrum of other objects lying at intermediate/high redshift, like quasars/AGN (Pitman et al. 2000; Maiolino et al. 2001; Hopkins et al. 2004) and GRB-host galaxies (e.g. GRB 020813 at  $z = 1.255$ , Savaglio & Fall 2004). On the other hand, a UV bump seems to be detected in the composite absorption spectrum of 96 intervening Mg II

systems at  $0.2 < z < 2.2$  (Malhotra 1997). However, Khare et al. (2005) come to an opposite conclusion for the composite absorption spectrum of 815 intervening QSO absorbers at  $1 \lesssim z \lesssim 1.9$ . Further evidence for MW-type dust being also present at high redshift comes from a composite spectrum of nine radio galaxies at  $z \sim 2.5$  (Vernet et al. 2001), and from the individual absorption spectra of three intervening Mg II absorbers at  $1.4 \lesssim z \lesssim 1.5$  (Wang et al. 2004).

It is not clear when star-forming galaxies at high redshift exhibit an extinction curve with a 2175 Å bump. Therefore, we have selected a sample of 34 UV-luminous galaxies at  $2 < z < 2.5$  from the FORS Deep Field spectroscopic survey (Noll et al. 2004; see Sect. 2). We will characterise their composite extinction curve at rest-frame UV wavelengths in terms of far-UV slope and presence/absence of the UV bump. The UV-luminous galaxies at  $z \sim 2$  exhibit large values of UV continuum reddening (e.g. van Dokkum et al. 2003; Daddi et al. 2004; Noll et al. 2004), if the slopes of their rest-frame UV continuum spectra are interpreted as for local starburst galaxies (Meurer et al. 1999; Calzetti et al. 2000; Leitherer et al. 2002). In this case, one can obtain attenuation factors at 1500 Å up to  $\sim 10^2$  (Noll et al. 2004), that are more than one order of magnitude larger than those determined for nearby starbursts, and correspond to the largest values estimated for LBGs at  $z \sim 3$  by Vijh et al. (2003). At variance with those LBGs at  $z \sim 3$ , the UV-luminous galaxies at  $z \sim 2$  are characterised by half-light radii of several kpc, total stellar masses between a few  $10^{10}$  and more than  $10^{11} M_\odot$ , metallicity between the LMC one and solar, and the absence of significant Ly $\alpha$  emission (Mehlert et al. 2002; Daddi et al. 2004; Noll et al. 2004; Shapley et al. 2004; Steidel et al. 2004; van Dokkum et al. 2004; Drory et al. 2005). Hence, the properties of the mixture of dust grains present in UV-luminous galaxies at  $z \sim 2$  may differ from those of LBGs at  $z \sim 3$  and those of local starburst galaxies.

In the following we illustrate this by making use of a new parametric description of the rest-frame UV SED that allows us to define dust-sensitive diagnostic diagrams. We interpret the distribution of the FDF sample galaxies in each of these diagrams through a comparison with that obtained either for a local reference sample of starburst galaxies or for models of starburst galaxies combining stellar population synthesis and radiative transfer calculations (Sect. 3).

Throughout this paper  $H_0 = 70 \text{ km s}^{-1} \text{ Mpc}^{-1}$ ,  $\Omega_\Lambda = 0.7$ , and  $\Omega_M = 0.3$  are adopted.

## 2. The spectroscopic sample: selection and data

### 2.1. The FORS sample of UV-luminous galaxies at $z \sim 2$

We have selected 34 galaxies (see Table 1) with  $I_{\text{Vega}} \lesssim 24.5$  in the spectroscopic-redshift range  $2 < z < 2.5$  from the catalogue of the FORS Deep Field (FDF) spectroscopic survey (Noll et al. 2004). The redshift interval chosen guarantees the covering of the rest-frame UV wavelength range from Ly $\alpha$  to around 2500 Å, including the 2175 Å feature, with the available optical spectroscopy. The limiting  $I$ -band magnitude prevents the contamination from faint Ly $\alpha$  emitters that were

<sup>1</sup> The LMC and SMC are deficient in heavy elements by factors of about 2.5 and 7, respectively, compared with the solar standard (Westerlund 1997).

**Table 1.** The spectroscopic sample of FDF galaxies at  $2 < z < 2.5$  (Noll et al. 2004). IDs, world coordinates, and total  $I$  magnitudes were taken from Heidt et al. (2003). Redshifts were derived by Noll et al. (2004). Luminosities at 1500 Å were taken from the same source, though corrected for the modified cosmology used.

No. (FDF)	RA (J2000)	Dec (J2000)	$I_{\text{Vega}}$ [mag]	$z$	$\log L_{1500}$ [W/Å]
1208	01 05 51.9	-25 48 04	23.68	2.178	33.88
1691	01 05 53.7	-25 45 29	23.89	2.344	33.94
1744	01 05 53.9	-25 46 06	24.10	2.374	33.91
1991	01 05 54.8	-25 46 16	24.33	2.334	33.85
2274	01 05 55.9	-25 44 34	23.34	2.253	34.18
2418	01 05 56.4	-25 45 12	23.16	2.332	34.25
2495	01 05 56.7	-25 43 44	23.31	2.453	34.25
2636	01 05 57.3	-25 44 02	23.43	2.253	34.01
3005	01 05 58.6	-25 48 14	23.51	2.253	34.03
3163	01 05 59.2	-25 45 38	23.35	2.441	34.21
3300	01 05 59.6	-25 46 30	23.91	2.375	34.07
3374	01 05 59.9	-25 45 11	23.34	2.386	34.27
3688	01 06 00.9	-25 47 05	24.07	2.375	34.00
3810	01 06 01.3	-25 45 28	22.67	2.372	34.44
3874	01 06 01.5	-25 45 46	23.30	2.483	34.23
3875	01 06 01.5	-25 47 34	24.53	2.243	33.84
3958	01 06 01.8	-25 44 29	23.87	2.130	33.97
4795	01 06 04.8	-25 47 14	23.31	2.159	34.13
4871	01 06 05.1	-25 46 04	23.39	2.472	34.26
4996	01 06 05.5	-25 46 28	23.25	2.028	34.04
5058	01 06 05.7	-25 46 26	23.34	2.027	34.15
5135	01 06 06.0	-25 44 44	23.62	2.346	34.02
5165	01 06 06.1	-25 44 43	23.26	2.346	34.34
5190	01 06 06.1	-25 44 43	24.39	2.347	33.83
5227	01 06 06.3	-25 43 52	23.85	2.399	34.08
6024	01 06 09.2	-25 48 14	22.00	2.372	34.68
6372	01 06 10.5	-25 48 29	23.38	2.349	34.21
6407	01 06 10.6	-25 45 32	23.59	2.162	33.95
6934	01 06 12.4	-25 44 57	22.90	2.445	34.43
6947	01 06 12.4	-25 48 15	23.83	2.357	33.97
7029	01 06 12.7	-25 45 58	23.63	2.374	34.12
7078	01 06 12.8	-25 46 01	23.97	2.378	34.00
7307	01 06 13.6	-25 47 25	24.07	2.438	34.01
7342	01 06 13.7	-25 46 13	23.80	2.375	34.06

discovered serendipitously. With an average luminosity at 1500 Å (rest frame)  $\langle L_{1500} \rangle = 1.4 \times 10^{34} \text{ W/Å}$  (not corrected for dust attenuation), the present sample of 34 galaxies represents the bright end of the distribution in  $L_{1500}$  of FDF galaxies at  $z \sim 2$  (see Fig. 1). Hereafter it is referred to as the FDF sample of “ $z \sim 2$  UV-luminous galaxies”.

The VLT-FORS spectra of our sample galaxies were obtained with the grism 150 I and a 1'' slit width (Noll et al. 2004), resulting in a measured spectral resolution element between 18 and 23 Å that corresponds to rest-frame 5 to 8 Å. The spectra cover the entire optical wavelength range providing reasonable data between 3500 and 9300 Å (observed frame), which allows us to probe the UV SED between 1216 Å (i.e. the Ly $\alpha$  transition of hydrogen) and  $\sim 2500$  Å, bracketing the region of the UV bump. Typical exposure times of about 10 h led to an average signal-to-noise ratio  $S/N$  of about 13 for the programme galaxies (see Noll et al. 2004). The quality of the spectra is

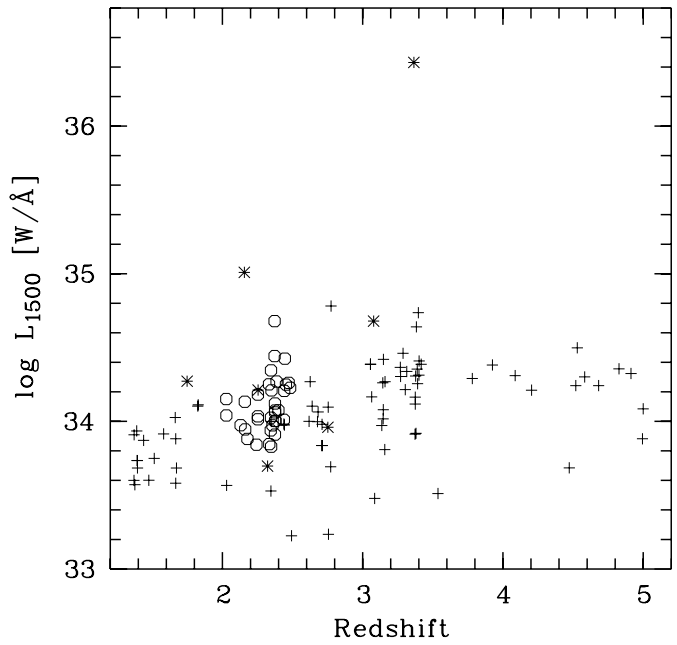


**Fig. 1.** The luminosity at 1500 Å (rest frame)  $L_{1500}$  as a function of redshift for the 118 galaxies at  $z > 1.35$  in the FDF spectroscopic sample (from Noll et al. 2004). The 34 galaxies under study (see Table 1) are reproduced with circles. Among the remaining high-redshift objects, star-forming galaxies are marked by crosses and QSOs by asterisks.  $L_{1500}$  refers to the measured emission within the rest-frame wavelength range from 1480 to 1520 Å.

sufficiently high for the purpose of this study. The spectra used are  $S/N$  optimised co-added, flux calibrated (including a correction for slit losses), and corrected for Galactic extinction ( $E_{B-V} = 0.018$ , Schlegel et al. 1998) using the CCM MW extinction law. Finally, the atmospheric B and A absorption bands were removed from the observed spectra using an empirical band model. The final spectra are slightly contaminated by a second order spectrum for  $\lambda > 6500$  Å. This effect does not significantly influence our study of the rest-frame UV continuum; the resulting relative flux uncertainty are not greater than 2 to 3% in the UV-bump region for the selected galaxies.

## 2.2. The IUE sample of nearby starbursts

In order to test our new parametric description of the rest-frame UV SED of star-forming galaxies, we select a sample of 24 well-known local starburst galaxies ( $z \lesssim 0.02$ ; see Table 2) with available UV spectra (see Kinney et al. 1993; Calzetti et al. 1994; Heckman et al. 1998). For this sample of nearby starbursts the luminosities at 1500 Å are typically one order of magnitude fainter than those of the FDF galaxies (cf. Leitherer et al. 2002 and Noll et al. 2004).

The UV spectra of this reference spectroscopic sample are taken from the INES archive of IUE newly-extracted spectra. The resolution element of the low-resolution IUE spectra is about 6 Å, i.e. similar to that achieved for the rest-frame UV spectra of the FDF sample of  $z \sim 2$  UV-luminous galaxies (see Sect. 2.1). A fine adjustment of the resolution of the IUE spectra was not needed, since this study focuses on the

**Table 2.** The comparison sample of local starburst galaxies having IUE spectra with suitable S/N and spectral coverage. The (activity) class parameter shown is taken from Kinney et al. (1993) with the exception of IRAS 08339+6517 and NGC 1741, for which this parameter comes from Leitherer et al. (2002) and Johnson et al. (1999), respectively. The meaning of the different parameters is as follows: BC(D)G = blue compact (dwarf) galaxy; Sy 2 = Seyfert 2 galaxy; SB nuc. = galaxy experiencing a starburst in its nucleus; Hs = hot spot galaxy; Lin = LINER; H II = galaxy with a spectrum typical of a H II region. All redshifts are taken from the NASA/IPAC Extragalactic Database (NED). Values of  $E_{B-V}$  were calculated using the maps of Galactic dust IR emission of Schlegel et al. (1998). The oxygen abundances O/H = 12 + log(O/H) are taken from Heckman et al. (1998) and complemented by data from Leitherer et al. (2002), Calzetti et al. (1994), and Johnson et al. (1999).

Name	Class	$z$	$E_{B-V}$ [mag]	O/H
ESO 338-4	BCG	0.0096	0.09	8.1
IZw 18	BCDG	0.0025	0.03	7.2
IRAS 08339+6517	H II	0.0191	0.09	8.7
Mrk 33	BCDG	0.0049	0.01	8.4
NGC 1097	Hs + Lin	0.0043	0.03	9.3
NGC 1313	H II	0.0016	0.11	8.4
NGC 1510	BCDG	0.0030	0.01	7.9
NGC 1705	BCDG	0.0021	0.01	8.0
NGC 1741	H II	0.0137	0.05	8.1
NGC 2782	SB nuc.	0.0085	0.02	8.8
NGC 3049	SB nuc.	0.0050	0.04	9.1
NGC 3353	BCDG	0.0031	0.01	8.4
NGC 3738	H II	0.0008	0.01	8.4
NGC 4214	SB nuc.	0.0010	0.02	8.2
NGC 4385	SB nuc.	0.0071	0.02	8.7
NGC 4449	H II	0.0007	0.02	8.4
NGC 4670	BCDG	0.0036	0.01	8.2
NGC 4861	BCDG	0.0028	0.01	8.0
NGC 6052	SB nuc.	0.0157	0.08	8.6
NGC 7496	Sy 2 + H II	0.0055	0.01	9.0
NGC 7673	H II	0.0114	0.04	8.5
NGC 7714	SB nuc.	0.0093	0.05	8.7
NGC 7793	H II	0.0008	0.02	8.6
UGC 9560	BCDG	0.0041	0.01	8.2

analysis of the UV continuum. Further selection criteria are as follows. First, all galaxies with a dominant young stellar population and available large  $10'' \times 20''$  aperture, low-resolution UV spectra at short *and* long wavelengths were selected. In fact, only the combined spectrum obtained from the spectra taken with the short-wavelength prime camera (SWP) and the long-wavelength prime and redundant cameras (LWP and/or LWR) cover the wavelength range between 1150 and 3350 Å, bracketing the region of the 2175 Å feature. Second, only those galaxies with spectra of suitable quality all over the UV spectral range were selected further. For obvious reasons, the data quality at the overlapping region of the two IUE spectral channels at around 2000 Å turned out to be a crucial parameter. Hence, combined spectra exhibiting a break in this overlapping region, usually with rather poor S/N, were rejected. As a result, the combined spectra of the 24 selected IUE starbursts exhibit an average S/N of about 10 between 2000 and 2350 Å, the final

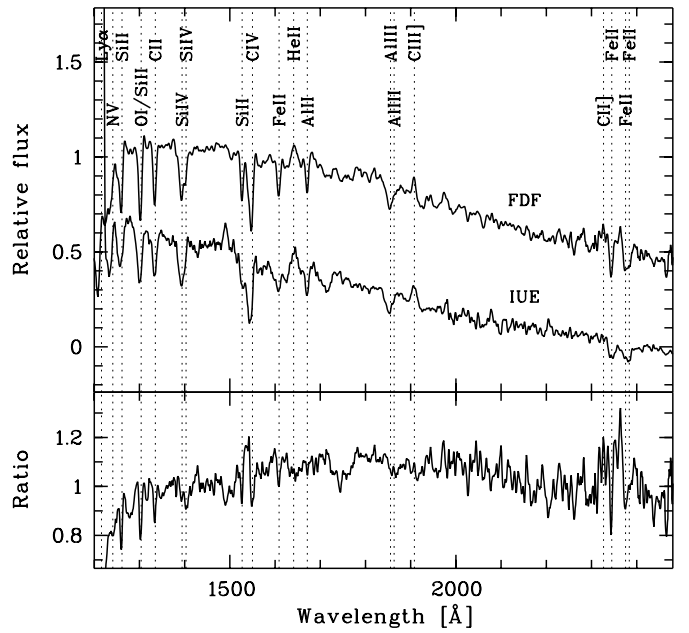


**Fig. 2.** Composite of 34 FDF galaxy spectra with  $S/N \geq 4$  in the range  $2 < z < 2.5$  (upper spectrum in the upper panel) in comparison with a composite of 24 IUE spectra of local galaxies (lower spectrum in the upper panel; offset by -0.5 for clarity). The lower panel gives the ratio of the FDF and the IUE composite spectrum. The positions of prominent UV lines are indicated. The Ly $\alpha$  line of the IUE composite is strongly affected by emission from the geocorona.

spectrum of each object being composed of all single spectra of sufficient S/N. In particular, the flux levels in the short and long wavelength spectra were adjusted in the wavelength range between 1850 Å and 1980 Å. Finally, the combined spectra were corrected for Galactic extinction and mapped into the rest frame.

The correction for Galactic extinction makes use of the maps of Galactic dust emission at IR wavelengths (Schlegel et al. 1998) for the derivation of realistic values for  $E_{B-V}$ , and of the CCM Milky Way extinction law for  $R_V = 3.1$ . This step is crucial, since the MW extinction law for the average ISM exhibits a relatively strong UV bump, so that small errors in  $E_{B-V}$  can lead to important uncertainties in the evaluation of the UV bump strength from the spectra of the 24 selected IUE starbursts. However, for the sample galaxies,  $E_{B-V}$  ranges between 0.01 and 0.11, with an average value of 0.03 (see Table 2), so that the effect of the correction for Galactic extinction on most of the spectra is possibly minimised.

### 2.3. Basic properties of the FDF and IUE samples

Figure 2 reproduces the composite spectrum of the 34 UV-luminous FDF galaxies at  $2 < z < 2.5$  and the composite spectrum of the 24 local IUE starbursts. These composite spectra were calculated according to the recipe given in Noll et al. (2004). This means that the rest-frame spectra were first normalised to a common mode in the range 1250 to 1500 Å and then averaged using equal weights.

**Table 3.** Properties of the composite spectra of the FDF  $2 < z < 2.5$  and the IUE local galaxy sample in comparison. The table lists the number of spectra averaged, the mean redshift, the mean equivalent width of six low-ionisation interstellar absorption lines (see Noll et al. 2004), and the EWs of C IV  $\lambda\lambda 1548, 1550$ , He II  $\lambda 1640$ , and C III]  $\lambda\lambda 1907, 1909$ . Emission lines have negative EWs. All errors given are mean errors.

Sample	FDF	IUE
$N$	34	24
$z$	$2.32 \pm 0.02$	$0.006 \pm 0.001$
$W_{\text{LIS}} [\text{\AA}]$	$1.97 \pm 0.09$	$1.89 \pm 0.08$
$W_{\text{CIV}} [\text{\AA}]$	$3.80 \pm 0.16$	$3.46 \pm 0.37$
$W_{\text{HeII}} [\text{\AA}]$	$-1.42 \pm 0.16$	$-2.06 \pm 0.45$
$W_{\text{CIII}]} [\text{\AA}]$	$-1.09 \pm 0.18$	$-1.91 \pm 0.23$

Wavelength regions affected by residuals of strong night sky lines or other defects were excluded from the averaging.

The lower panel of Fig. 2 shows the ratio of the FDF and IUE composites. In general, both rest-frame UV spectra are very similar, and show clear signatures of the dominance of young stellar populations. For a large wavelength range the continuum flux increases towards shorter wavelengths. However, for  $\lambda < 1800 \text{ \AA}$  the FDF composite is distinctly flatter than the IUE composite. Conversely, for  $\lambda > 1800 \text{ \AA}$  the local starburst composite shows a flatter slope than the other. We will discuss these behaviours in the following sections.

In addition to the overall UV continua, the average equivalent width of six prominent low-ionisation lines ( $W_{\text{LIS}}$ , see Shapley et al. 2003; Noll et al. 2004) are similar between the two samples (Fig. 2 and Table 3). In fact,  $W_{\text{LIS}} = 1.97 \pm 0.09 \text{ \AA}$  for the FDF composite and  $1.89 \pm 0.08 \text{ \AA}$  for the local one. The quoted errors include statistical uncertainties and the variance of the line strengths within each sample (see Noll et al. 2004). These low-ionisation lines originate in the intervening neutral interstellar medium between the OB stars (responsible of the rest-frame UV continuum) and the observer. Due to their high saturation, these lines are barely sensitive to chemical abundances. Hence, they primarily trace the spatial and velocity distribution of the neutral interstellar gas illuminated by the rest-frame UV continuum. Therefore,  $W_{\text{LIS}}$  is a measure of the product of the neutral clouds' covering fraction and the velocity spread. According to Shapley et al. (2003) differences in  $W_{\text{LIS}}$  are mainly due to variations in the covering fraction.

Comparable equivalent widths are also obtained for the important high-ionisation C IV doublet:  $3.80 \pm 0.14 \text{ \AA}$  for the FDF sample, and  $3.46 \pm 0.37 \text{ \AA}$  for the IUE sample. The C IV equivalent width mainly measures the strength of winds from hot, massive and, thus, young stars and is a good metallicity indicator (Leitherer et al. 2001). Using C IV Mehlert et al. (2002)<sup>2</sup> estimated an average metallicity of  $Z \approx 0.42 Z_{\odot}$  for an analogous sample of FDF galaxies at  $2 < z < 2.5$ . Measuring the purely photometric indices “1370” and “1425” (Leitherer et al. 2001) in medium-resolution spectra of two  $z \sim 2$  FDF galaxies

<sup>2</sup> The EWs of C IV listed in Mehlert et al. (2002) are on average about 20% larger than in this study. This is due to a wider wavelength range to derive the continuum level (190  $\text{\AA}$  instead of  $\sim 80 \text{ \AA}$ ) and an automatic instead of interactive measurement technique.

Mehlert et al. (2005) find indications for even higher metallicities close to the solar value. A similar metallicity as the C IV based of the FDF galaxies (assuming the solar oxygen abundance  $(\text{O/H})_{\odot} = 8.93$ ) we find for our IUE sample of nearby starbursts having  $\langle \text{O/H} \rangle \approx 8.6$  (see Table 2 and, e.g., Heckman et al. 1998).

In addition to the P Cygni profiles of high-ionisation lines such as C IV, the detection of the He II and C III] emission features indicates the presence of a significant population of young, very massive stars in both samples (Fig. 2 and Table 3). In particular, the He II line emission is essentially produced by Wolf-Rayet stars (Schaerer 2003), whereas the C III] line emission has a nebular origin, and traces the electron temperature of H II regions (see Heckman et al. 1998).

### 3. Analysis

In this study we compare diagnostics measured on the rest-frame UV spectra of the 34 FDF sample galaxies (see Sect. 2.1) with those determined on the rest-frame UV SEDs of models of starburst galaxies. This procedure is analogous to that adopted by Gordon et al. (1997) for the analysis of the dust properties for the Calzetti et al. (1994) sample of nearby starbursts. In addition, we use the IUE sample of 24 local starbursts (see Sect. 2.2) as a further comparison. Here we illustrate both the models and the diagnostics adopted in this study. Furthermore, we demonstrate that the new diagnostics tailored to the FORS data lead to the same conclusions as those of Gordon et al. (1997) when applied to the IUE sample.

#### 3.1. Modelling the UV continuum of starburst galaxies

We produce synthetic SEDs for starburst galaxies by combining stellar population synthesis models with models of radiative transfer of the stellar and scattered radiation through the dusty ISM.

##### 3.1.1. Stellar population synthesis models

Intrinsic (i.e. non attenuated by dust) SEDs for starburst galaxies are derived from the stellar population synthesis code for the stellar continuum emission of Maraston (2005, M05)<sup>3</sup>. These models include the thermally pulsating asymptotic giant branch phase for intermediate-mass ( $2-5 M_{\odot}$ ) stars, at variance with all others (e.g. Fioc & Rocca-Volmerange 1997, FR97; Leitherer et al. 1999; Bruzual & Charlot 2003, BC03). However, this relevant difference does not affect any of the results reported here, since the SEDs produced for analogous models of M05, BC03, and FR97 do not differ significantly in shape at rest-frame UV wavelengths (see, e.g., Fig. 14 in M05). This is also shown in Table 5 of Sect. 3.2.2. Finally, we note that the spectral resolution of the M05 models ( $\Delta\lambda = 10 \text{ \AA}$ ) matches reasonably well those of the rest-frame UV continua of the FDF sample galaxies, as given by the FORS spectra

<sup>3</sup> The Maraston (2005) models are available at <http://www-astro.physics.ox.ac.uk/~maraston/>

( $\Delta\lambda = 5\text{--}8 \text{\AA}$ ), and of the nearby starbursts observed with IUE ( $\Delta\lambda = 6 \text{\AA}$ ).

In Sect. 2.3, we have shown that there is evidence for the  $z \sim 2$  UV-luminous FDF galaxies being both actively forming stars and metal enriched ( $\langle Z \rangle \gtrsim 0.4 Z_{\odot}$ ). In addition, starburst galaxies in the nearby and distant universe seem to undergo multiple star-formation episodes of a few 10 Myr to several 100 Myr (Calzetti 1997; Shapley et al. 2001; van Dokkum et al. 2004). Therefore, we adopt composite stellar populations models where the SFR is constant with time, the metallicity is fixed and ranges between 2% and twice solar, and the time elapsed since the start of the star-formation activity (i.e. the age of the model) ranges between 5 and 500 Myr. As a reference, we compute additional simple stellar population models spanning the same metallicity range as for the previous models but with ages between 5 and 100 Myr. All these models assume a Salpeter (1955) initial mass function with an upper mass cut-off of  $100 M_{\odot}$ .

Given the measured metallicities (Mehlert et al. 2002, 2005) and the expected ages of the  $z \sim 2$  UV-luminous galaxies, in the following analysis we will make use mostly of M05 models with a continuous star-formation activity (i.e. with a SFR  $e$ -folding time  $\tau = 10$  Gyr) along 50, 200, or 500 Myr, and metallicities equal to 0.5 or  $1.0 Z_{\odot}$ . These models are also suitable to reproduce the properties of the IUE sample of nearby starbursts, though a few objects in the latter sample have  $Z < 0.1 Z_{\odot}$  (e.g. IZw 18) and a few others have significantly supersolar metallicity (see Table 2).

### 3.1.2. Radiative transfer models

We make use of the radiative transfer calculations for the SHELL dust/stars configuration of WG00 in order to describe the properties of dust attenuation for the galaxies under investigation. The reason is that the rather regular properties of dust attenuation in starburst galaxies of the local universe (Calzetti et al. 1994, 2000) may be reproduced by a model where a two-phase, clumpy, dusty medium is distributed in a shell surrounding the stars (Gordon et al. 1997). This dust/stars configuration is analogous to that adopted by Fischer et al. (2003) to give an independent physical explanation of the so-called “Calzetti law” (Calzetti et al. 1994, 2000) based on a turbulent ISM. According to Dopita et al. (2005), the pressure in the diffuse phase of the ISM (or, equivalently, its density), and the molecular-cloud dissipation timescale control the pan-spectral SED of starburst galaxies.

The WG00 radiative transfer models (including multiple scattering) are based on Monte Carlo calculations for a scale-free spherically-symmetric geometry (see also Gordon et al. 2001). In particular, the SHELL dust/stars configuration assumes the stars to be distributed inside an inner sphere with radius equal to 0.3 times the system radius, and the dust to be distributed inside a shell extending radially from 0.3 to 1 times the system radius. Dust can be distributed locally either in a homogeneous (i.e. diffuse) ISM, or in a two-phase, clumpy ISM. In the latter case, high-density clumps are embedded in a low-density interclump medium, the low-to-high-density ratio

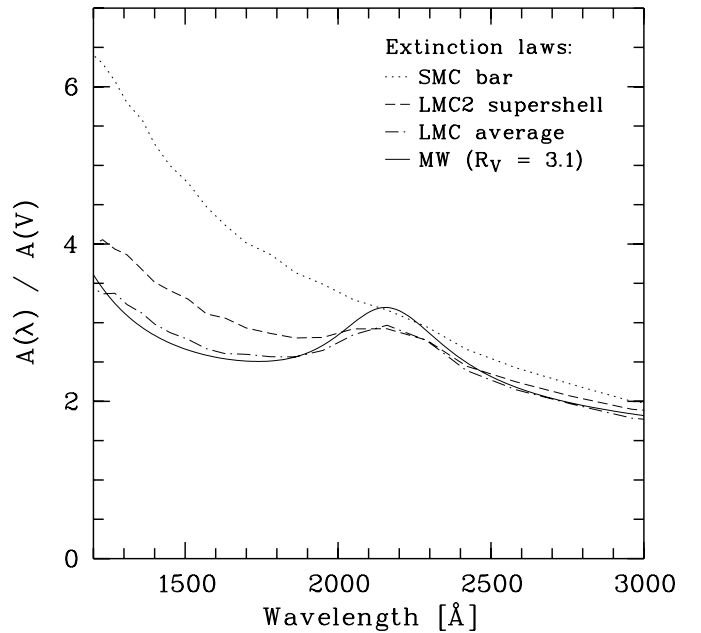


**Fig. 3.** Ratio of the attenuation factor  $A$  at the wavelength  $\lambda$  to the average attenuation in the  $V$  band as function of  $\lambda$  for different extinction laws. The CCM Milky Way extinction law is shown for  $R_V = A_V/E_{B-V} = 3.1$  as solid line. The LMC average, LMC 2 supershell, and SMC bar extinction laws (Gordon et al. 2003) are marked by dash-dotted, dashed, and dotted lines, respectively.

being equal to 0.01, with a filling factor of 0.15. Models are parameterised by the radial extinction optical depth from the centre to the edge of the dust environment at  $V$  band ( $\tau_V$ ), assuming a constant density homogeneous distribution,  $\tau_V$  ranging from 0.25 to 50. Finally, the mixture of dust grains can be characterised by an extinction curve that is typical either of the SMC or of the MW (see Fig. 3 and Sect. 1).

Hereafter, we illustrate a few aspects of these SHELL radiative transfer models for the non-specialist reader. Figure 4 shows the behaviour of the UV spectral slope  $\beta^4$ , as defined in Sect. 3.2.1, as a function of the attenuation (in mag) at  $1500 \text{\AA}$   $A_{1500}$  for different starburst models with age equal to 200 Myr and solar metallicity (cf. Sect. 3.1.1). The relation between  $\beta$  and  $A_{1500}$  is linear in case of a homogeneous dusty ISM, whatever the dust type. Conversely, it is non-linear for the two-phase, clumpy dust distribution. In the former case,  $\beta$  and  $A_{1500}$  increase at a constant rate because the angle-averaged optical depth at UV wavelengths increases monotonically with the dust column density (i.e.  $\tau_V$ ). In the latter case, first  $\beta$  and  $A_{1500}$  show a positive correlation because the optical depth at UV wavelengths of a clump increases with  $\tau_V$ . However, when the clumps become optically thick at UV wavelengths, the attenuation at these wavelengths is given by the simple blocking action of the clumps, while the UV radiation reaches the outside observer through the optically thin, diffuse component of the ISM. Hence,  $\beta$  stalls while  $A_{1500}$  keeps on increasing. When the angle-averaged optical depth at UV wavelengths of

<sup>4</sup> The non-ionising UV-flux density distribution of an observed star-forming galaxy is well reproduced by a power law  $f_{\lambda} \sim \lambda^{\beta}$ , where  $\beta$  is referred to as the UV slope (see, e.g., Calzetti et al. 1994).

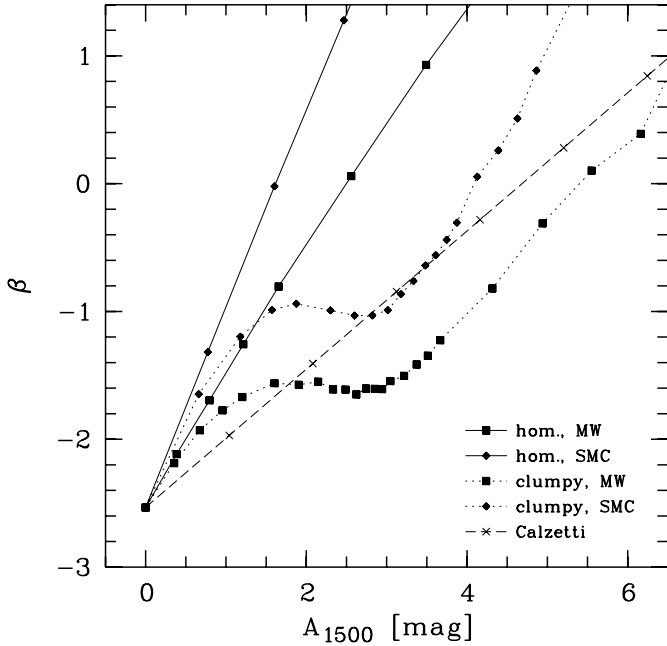


**Fig. 4.** The UV continuum slope  $\beta$  as a function of the attenuation at 1500 Å  $A_{1500}$  for different reddened model spectra. In all cases a M05 model with Salpeter IMF, continuous star-formation, an age of 200 Myr, and solar metallicity was combined with SHELL models of WG00 for different dust distribution, extinction laws, and optical depth. Different dust column densities are indicated by filled squares (MW dust) and lozenges (SMC dust), connected with solid (homogeneous model) and dashed lines (clumpy model), respectively. The symbols have been plotted for the average radial visual optical depth  $\tau_V = 0, 0.25, \dots, 1, 1.5, \dots, 6, 7, \dots, 10$ . The dash-dotted line refers to the Calzetti et al. (2000) attenuation law. The crosses are plotted in intervals of  $\Delta E_{B-V} = 0.1$ .

the diffuse component of the ISM tends to unity,  $\beta$  and  $A_{1500}$  increase together again. We note that, in case of a more realistic size and density distribution of the dusty clumps, one can expect a behaviour that is intermediate between those produced by the homogeneous and two-phase, clumpy dust distributions. Furthermore, Fig. 4 confirms that SMC-type dust produces a larger attenuation at UV wavelengths than MW-type dust, for fixed  $\tau_V$ , whatever the structure of the dusty ISM.

Finally, Fig. 4 shows that a linear relation between  $\beta$  and  $A_{1500}$  is expected when the empirical “Calzetti law” is assumed to hold, whatever the dust column density of the ISM. We remind that WG00 could achieve the best agreement with the “Calzetti law” for a two-phase, clumpy SHELL model with SMC dust, and  $\tau_V = 1.5$ .

### 3.2. A new parametric description of the UV continuum

#### 3.2.1. The parameter set

The UV SEDs of composite stellar population models can be parameterised with a power law ( $f(\lambda) \propto \lambda^\beta$ ), since the bulk radiation comes from the emission from hot stars in the Rayleigh-Jeans regime. This is so also true for observed UV SEDs of nearby starbursts (e.g. Calzetti et al. 1994), that are affected by dust attenuation (see footnote 4). The latter authors measured

**Table 4.** Wavelength windows for the derivation of the UV continuum slope parameters  $\beta$  and  $\gamma_1$  to  $\gamma_4$  using power-law fits.

Par.	Windows
$\beta$	1268–1284, 1309–1316, 1342–1371, 1435–1496, 1562–1583, 1677–1740
$\gamma_1$	1268–1284, 1309–1316, 1342–1371, 1435–1496
$\gamma_2$	1562–1583, 1677–1740, 1760–1833, 1866–1890
$\gamma_3$	1920–2050, 2070–2175
$\gamma_4$	2175–2310, 2400–2480

the UV slope  $\beta$  across the wavelength range 1200–2600 Å, with the exclusion of the wavelength region between 1950 and 2400 Å. By doing so, their  $\beta$  was not affected by the possible presence of dust characterised by an extinction law with the UV bump. Other analyses of the UV continuum properties of star-forming galaxies in the local and distant universe defined  $\beta$  across a narrower range, i.e. from 1200 to 1800 Å (Heckman et al. 1998; Leitherer et al. 2002; Noll et al. 2004), mostly owing to the missing spectral coverage at rest-frame  $\lambda > 2400$  Å. Following the previous authors we also measure  $\beta$  across the wavelength range 1200–1800 Å. The quality of the FORS spectra available for the 34 FDF galaxies at  $2 < z < 2.5$  is not good enough to provide a reliable fit at  $\lambda > 2400$  Å.

In addition to the “standard” parameter  $\beta$ , we define six new parameters, since the main interest of this study is to investigate if and when the UV bump is present among the FDF sample galaxies. The definition of four parameters (see Table 4) is based on power-law fits to sub-regions of the UV continuum as well as that of  $\beta$ . In particular, we divide the wavelength range between 1200 and 2500 Å in four sub-regions, delimited by the CIV doublet at 1550 Å, the CIII] emission feature at 1908 Å, and the centre of the UV bump at 2175 Å. Furthermore, we select windows within a given sub-region (see Table 4) in order to avoid that the presence of strong spectral lines produces a bias of the fit to the continuum. For  $\lambda < 1800$  Å we essentially adopt the windows defined by Calzetti et al. (1994), with the exception of the 1435–1496 Å window, which is taken from Leitherer et al. (2002). We call these four parameters  $\gamma_1$ ,  $\gamma_2$ ,  $\gamma_3$ , and  $\gamma_4$  after the progressive number of the four sub-regions, starting from that defined by the shortest wavelengths. Figure 5 reproduces the five power-law fits corresponding to the previous five parameters (i.e.  $\beta$  plus the four new slopes of the fits) for the composite spectrum of 34 UV-luminous FDF galaxies at  $z \sim 2$ . In addition, we introduce two parameters, i.e.  $\gamma_{12} = \gamma_1 - \gamma_2$  and  $\gamma_{34} = \gamma_3 - \gamma_4$ . The meaning of these two additional parameters is straightforward:  $\gamma_{12}$  measures the “curvature” of the spectral UV continuum across 1500 Å;  $\gamma_{34}$  measures the “curvature” of the spectral UV continuum across the UV bump (negative  $\gamma_{34}$  identify the presence of dust with an extinction law exhibiting the 2175 Å feature). The parameter  $\gamma_{34}$  does not represent the “strength” of the UV bump however. In fact, radiative transfer effects tend to dilute the prominence of the UV bump in the resulting attenuation function with respect to that in the extinction curve when the opacity increases, whatever the dust/stars configuration and the structure of the

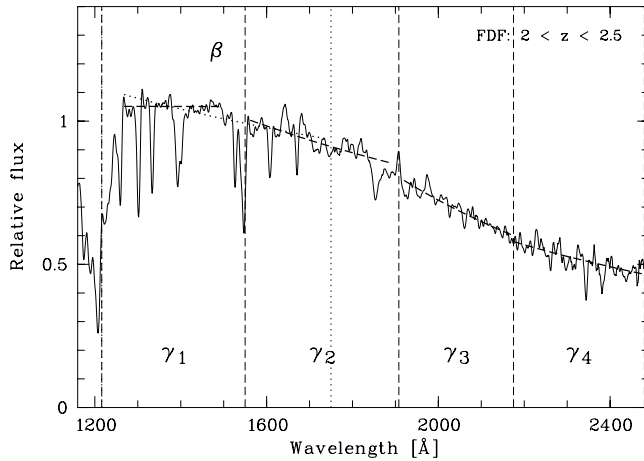


**Fig. 5.** Demonstration of the derivation of the UV continuum slopes  $\beta$  and  $\gamma_1$  to  $\gamma_4$  for the composite spectrum of 34 luminous FDF galaxies at  $2 < z < 2.5$  (cf. Fig. 2). The power law fits are shown as thick dotted ( $\beta$ ) and dashed ( $\gamma_1$  to  $\gamma_4$ ) curves. The limits for the fit ranges are indicated by vertical dotted ( $\beta$ ) and dashed ( $\gamma_1$  to  $\gamma_4$ ) lines.

dusty ISM, with the exception of a homogeneous SHELL configuration (Cimatti et al. 1997; WG00; Pierini et al. 2004).

### 3.2.2. Sensitivity of the parameters to properties of the stellar populations or of dust attenuation

The five parameters  $\beta$ , and  $\gamma_1$  to  $\gamma_4$  describe the observed UV SEDs of a galaxy and, thus, depend in a complex way on the properties of the stellar populations and of dust attenuation (see Sect. 3.1). Nevertheless, we can disentangle the principal dependencies of each parameter by investigating the behaviour of the five slopes, as obtained for the UV SEDs of a suite of starburst models, as a function of the model parameters.

In Fig. 6 we illustrate the effects on the UV continuum parameters  $\beta$  and  $\gamma_3$  of different metallicities and ages, for single-burst and continuous star-formation models of M05. A priori, one would expect that  $\gamma_3$  is particularly sensitive to very young ages and high metallicities, since it characterises the wavelength range from 1900 to 2175 Å. However,  $\gamma_3$  hardly changes for reasonable models of  $z \sim 2$  UV-luminous galaxies, with continuous star-formation, metallicity equal to 0.5 or  $1.0 Z_\odot$ , and ages higher than a few 10 Myr (see Sect. 3.1.1). The same conclusion holds for  $\beta$ : conspicuous changes in  $\beta$  would be possible only for single burst models with ages greater than 20 Myr. The latter models are not realistic, since they do not provide large UV luminosities long after the episode of star-formation activity. Furthermore, values of  $\beta > -2$  are produced by stellar population synthesis models with a SFR *e*-folding time as short as 1 Gyr only about 10 Gyr after the onset of the star-formation activity, i.e. at a time much longer than the age of the universe at  $z \sim 2$  (i.e.  $\sim 3$  Gyr). SFR *e*-folding times less than 1 Gyr can not justify the vigorous star-formation activity of the UV-luminous FDF galaxies at  $z \sim 2$  that is witnessed by the measured emission line EWs (see Table 3).

Table 5 lists typical values (see Sect. 3.1.1) for all five UV continuum slope parameters. In particular, it shows that  $\gamma_4$

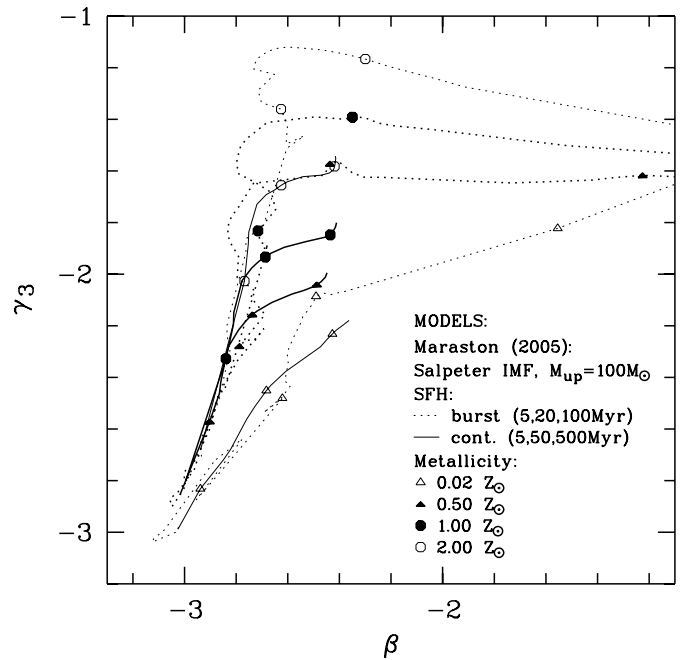


**Fig. 6.** The relation between the slope parameters  $\gamma_3$  and  $\beta$  for different M05 model spectra. The tracks plotted show the change of  $\beta$  and  $\gamma_3$  with increasing age ( $t \leq 1$  Gyr) for stellar population models differing in the star-formation history (single burst or continuous star-formation) as well as the metallicity (0.02, 0.5, 1.0, and  $2.0 Z_\odot$ ). For single burst models (dotted lines) symbols (see legend) are plotted for 5, 20, and 100 Myr. Ages of 5, 50, and 500 Myr are marked in case of models with continuous star-formation (solid lines). All tracks start at  $\beta \sim -3$  and  $\gamma_3 \sim -3$ .

exhibits only a minor dependence on the properties of the stellar populations, while  $\gamma_2$  is particularly sensitive to changes in metallicity and age. The latter is explained by the great number of spectral lines originated in the atmospheres of hot stars that fall within the wavelength range 1550 to 1900 Å, where  $\gamma_2$  is defined, and the sensitivity of the same wavelength range to the O-to-B-star number ratio. Finally, Table 5 shows that the slope parameters span a range  $\Delta\gamma$  of up to 0.5 in response to the variations in the properties of the stellar populations that are assumed to be reasonable for our sample galaxies. On the other hand, Table 5 shows that the different  $\gamma$  parameters characterising the rest-frame UV SED can change by up to 0.2 with respect to those obtained from the M05 models, when they are determined from intrinsic rest-frame UV SEDs taken from BC03 or FR97. Hence, the dependence of all the seven UV continuum slope parameters on the source of the stellar population synthesis code does not affect the study of the extinction law in UV luminous galaxies at  $z \sim 2$ .

Now, stellar population synthesis models do not include the absorption of UV light by interstellar gas, so that one may expect that the parameters listed in Table 5 are affected by systematic uncertainties. Therefore, we have computed semi-analytic spectra including line absorption by the ISM by combining the normalised, composite rest-frame UV spectrum of our high-redshift sample galaxies (Fig. 2) with the UV spectra of the M05 models listed in Table 5. As a result, we estimate that the deviations in the slope parameters listed there,

**Table 5.** Continuum slope parameters for continuous star-formation models of M05, differing in metallicity ( $0.5$  and  $1 Z_{\odot}$ ) and age (50 and 500 Myr), and for analogous models of BC03 and FR97.

Par.	$0.5 Z_{\odot}$	$1 Z_{\odot}$	$0.5 Z_{\odot}$	$1 Z_{\odot}$	Ref.
$\beta$	-2.74	-2.69	-2.49	-2.44	M05
$\gamma_1$	-2.80	-2.87	-2.41	-2.47	M05
$\gamma_2$	-2.23	-1.98	-2.00	-1.74	M05
$\gamma_3$	-2.16	-1.93	-2.04	-1.85	M05
$\gamma_4$	-3.04	-3.03	-2.92	-2.96	M05
$\beta$	-2.73	-2.67	-2.45	-2.39	BC03
$\gamma_1$	-2.83	-2.96	-2.40	-2.50	BC03
$\gamma_2$	-2.23	-1.86	-1.97	-1.60	BC03
$\gamma_3$	-2.07	-1.75	-1.95	-1.68	BC03
$\gamma_4$	-3.00	-3.01	-2.88	-2.95	BC03
$\beta$	-2.61	-2.58	-2.36	-2.33	FR97
$\gamma_1$	-2.58	-2.70	-2.19	-2.31	FR97
$\gamma_2$	-2.24	-1.94	-2.01	-1.71	FR97
$\gamma_3$	-2.11	-1.85	-2.00	-1.79	FR97
$\gamma_4$	-2.85	-2.88	-2.76	-2.84	FR97

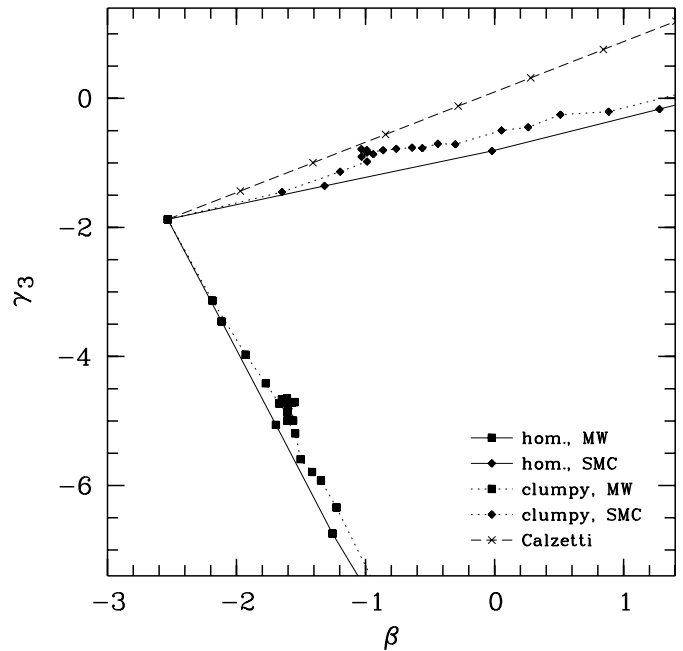


**Fig. 7.** The relation between the slope parameters  $\gamma_3$  and  $\beta$  for different reddened model spectra. The line types and symbols are as in Fig. 4.

as produced by interstellar line-absorption, are typically about 0.1. This very small effect is also a consequence of the careful selection of wavelength windows excluding strong interstellar lines, where the five UV continuum slope parameters are defined (see Fig. 2).

Finally, we discuss how the latter parameters depend on the properties of dust attenuation, for the models discussed in Sect. 3.1.2. In particular, we illustrate the behaviour of dusty, star-forming galaxies with a solar metallicity, 200 Myr-old composite stellar population in the  $\beta - \gamma_3$  plane (see Fig. 7) already introduced (see Fig. 6). In this diagram, the loci of models with MW and SMC dust are clearly separated, whatever  $\tau_V$ . The slope parameters  $\gamma_3$  and  $\beta$  of the two models differ by more than 1.6 and 0.5, respectively, already for  $\tau_V \gtrsim 0.25$ . Furthermore,  $\gamma_3 \sim -2$  is a delimiter of the regions populated by the models for MW-like and SMC-like dust. Hence, the distribution in the  $\beta - \gamma_3$  plane can reveal the presence of dust with an extinction law exhibiting the UV bump already for low values of the dust column density. On the other hand, it is not particularly sensitive to the structure of the dusty ISM. As a reference, Fig. 7 reproduces additional models with the same stellar populations as the others but where dust attenuation follows the Calzetti et al. (2000) attenuation law. As expected (Gordon et al. 1997), the latter models show a similar behaviour to those with a SHELL configuration of SMC-type dust distributed in a two-phase, clumpy medium.

In conclusion, the five UV continuum slopes defined in this study are proved to be much more sensitive to the characteristic extinction law (i.e. to the properties of the mixture of the dust grains) of the system, than to those of the stellar populations present in the system, for a fixed dust/stars distribution. Conversely, they cannot constrain the structure of the dusty ISM.

### 3.2.3. A test for the method: the IUE sample of nearby starbursts

Here we test the reliability of our method of investigating the presence of dust with an extinction law exhibiting the 2175 Å bump, that is based on a new parametric approach. We do so by investigating the slope parameters defined in Sect. 3.2.1 of our IUE sample of nearby starbursts (see Sect. 2.2) with respect to models. Table 6 lists the parameters measured by us for this reference sample. Composite stellar populations models are calculated as in M05 for a standard Salpeter IMF, a continuous star-formation activity along 50 or 500 Myr, and a metallicity equal to  $0.5 Z_{\odot}$  or  $1.0 Z_{\odot}$ . Furthermore, the properties of dust attenuation are described through the two-phase, clumpy SHELL dust/stars configuration of WG00 for SMC-like or MW-like dust, where the average opacity of the dust shell is a free parameter.

The combined slope parameter  $\gamma_{34}$  is most suitable to study the presence of the 2175 Å feature. This is illustrated by the plot of  $\gamma_{34}$  versus  $\beta$  in Fig. 8 which shows that models with different composite stellar populations and SMC-type dust, lacking the 2175 Å feature, exhibit  $\gamma_{34} \sim 1$ , whatever  $\tau_V$  and  $\beta$ , respectively. Conversely,  $\gamma_{34}$  rapidly decreases below zero when  $\beta$  increases for models where UV-bump producing MW-type dust is present (see Fig. 3). Now, the 24 local starbursts of the IUE sample are distributed in a region delimited by  $-2.5 < \beta < 0.5$  and  $-3 < \gamma_{34} < 3$ . The bulk of these galaxies populates a region of the  $\beta - \gamma_{34}$  plane that is confined by the model curves, for  $\beta > -3$ . Our interpretation is that these nearby starbursts possibly contain relatively small amount of dust with an extinction law exhibiting only a modest UV bump, if any. Moreover, analysing the distributions of the other slope parameters (see Fig. 9) we find that the far-UV uprise of the extinction law is intermediate between those of the SMC and MW. These are

**Table 6.** UV continuum slope parameters of our IUE sample of 24 local starburst galaxies (see Table 2).

Name	$\beta$	$\gamma_1$	$\gamma_2$	$\gamma_3$	$\gamma_4$	$\gamma_{12}$	$\gamma_{34}$
ESO 338-4	$-1.19 \pm 0.09$	$+0.02 \pm 0.08$	$-1.06 \pm 0.07$	$-1.55 \pm 0.09$	$-3.01 \pm 0.07$	$+1.08 \pm 0.11$	$+1.46 \pm 0.11$
IZw 18	$-1.80 \pm 0.07$	$-1.20 \pm 0.06$	$-2.05 \pm 0.06$	$-2.91 \pm 0.23$	$-3.83 \pm 0.22$	$+0.86 \pm 0.08$	$+0.92 \pm 0.32$
IRAS 08339+6517	$-0.63 \pm 0.08$	$+0.16 \pm 0.07$	$-1.45 \pm 0.09$	$-2.15 \pm 0.14$	$+0.29 \pm 0.13$	$+1.61 \pm 0.11$	$-2.44 \pm 0.19$
Mrk 33	$-0.95 \pm 0.09$	$-1.30 \pm 0.07$	$-0.48 \pm 0.11$	$-1.39 \pm 0.14$	$-0.76 \pm 0.07$	$-0.82 \pm 0.13$	$-0.63 \pm 0.16$
NGC 1097	$-0.37 \pm 0.13$	$-0.75 \pm 0.12$	$+0.77 \pm 0.12$	$+0.91 \pm 0.17$	$-0.65 \pm 0.15$	$-1.51 \pm 0.17$	$+1.56 \pm 0.23$
NGC 1313	$-1.21 \pm 0.19$	$-0.58 \pm 0.20$	$-0.87 \pm 0.14$	$-3.33 \pm 0.28$	$-1.72 \pm 0.22$	$+0.29 \pm 0.24$	$-1.61 \pm 0.36$
NGC 1510	$-1.25 \pm 0.08$	$-0.62 \pm 0.07$	$-0.92 \pm 0.08$	$-1.54 \pm 0.17$	$-1.74 \pm 0.14$	$+0.30 \pm 0.10$	$+0.21 \pm 0.22$
NGC 1705	$-2.36 \pm 0.04$	$-2.10 \pm 0.04$	$-2.13 \pm 0.06$	$-1.91 \pm 0.05$	$-3.56 \pm 0.05$	$+0.03 \pm 0.07$	$+1.65 \pm 0.07$
NGC 1741	$-0.16 \pm 0.13$	$+1.15 \pm 0.11$	$-0.64 \pm 0.11$	$-0.71 \pm 0.14$	$-2.58 \pm 0.18$	$+1.79 \pm 0.16$	$+1.87 \pm 0.23$
NGC 2782	$-0.79 \pm 0.12$	$-0.36 \pm 0.11$	$-0.50 \pm 0.10$	$+0.31 \pm 0.24$	$-0.07 \pm 0.26$	$+0.14 \pm 0.14$	$+0.38 \pm 0.35$
NGC 3049	$-1.23 \pm 0.12$	$-0.65 \pm 0.08$	$-0.43 \pm 0.12$	$-2.20 \pm 0.27$	$-0.94 \pm 0.17$	$-0.22 \pm 0.14$	$-1.27 \pm 0.32$
NGC 3353	$-0.84 \pm 0.07$	$-0.37 \pm 0.07$	$-1.42 \pm 0.06$	$-2.50 \pm 0.21$	$-1.68 \pm 0.15$	$+1.05 \pm 0.09$	$-0.82 \pm 0.26$
NGC 3738	$-1.47 \pm 0.07$	$-0.94 \pm 0.06$	$-1.11 \pm 0.05$	$-0.97 \pm 0.14$	$-2.06 \pm 0.12$	$+0.17 \pm 0.08$	$+1.09 \pm 0.18$
NGC 4214	$-0.98 \pm 0.05$	$-0.24 \pm 0.04$	$-1.20 \pm 0.03$	$-1.07 \pm 0.07$	$-2.35 \pm 0.06$	$+0.97 \pm 0.05$	$+1.29 \pm 0.10$
NGC 4385	$-0.16 \pm 0.12$	$+0.10 \pm 0.12$	$-0.88 \pm 0.09$	$+0.06 \pm 0.14$	$-2.88 \pm 0.12$	$+0.98 \pm 0.15$	$+2.94 \pm 0.18$
NGC 4449	$-1.31 \pm 0.05$	$-0.56 \pm 0.03$	$-1.19 \pm 0.04$	$-1.21 \pm 0.09$	$-3.56 \pm 0.09$	$+0.63 \pm 0.05$	$+2.35 \pm 0.12$
NGC 4670	$-1.23 \pm 0.06$	$-0.97 \pm 0.05$	$-1.45 \pm 0.05$	$-0.21 \pm 0.09$	$-1.77 \pm 0.07$	$+0.49 \pm 0.07$	$+1.56 \pm 0.12$
NGC 4861	$-2.03 \pm 0.05$	$-1.54 \pm 0.05$	$-2.00 \pm 0.05$	$-2.28 \pm 0.07$	$-2.30 \pm 0.07$	$+0.45 \pm 0.07$	$+0.01 \pm 0.10$
NGC 6052	$+0.39 \pm 0.18$	$+2.38 \pm 0.15$	$-0.91 \pm 0.13$	$-0.53 \pm 0.18$	$-1.47 \pm 0.14$	$+3.29 \pm 0.20$	$+0.94 \pm 0.23$
NGC 7496	$-1.07 \pm 0.12$	$-1.26 \pm 0.10$	$+0.19 \pm 0.11$	$-3.71 \pm 0.15$	$-0.97 \pm 0.10$	$-1.45 \pm 0.14$	$-2.74 \pm 0.18$
NGC 7673	$-0.96 \pm 0.09$	$-0.50 \pm 0.09$	$-0.63 \pm 0.08$	$-2.29 \pm 0.16$	$-2.05 \pm 0.11$	$+0.13 \pm 0.12$	$-0.24 \pm 0.20$
NGC 7714	$-0.95 \pm 0.05$	$-0.90 \pm 0.04$	$-0.37 \pm 0.05$	$-2.29 \pm 0.16$	$-1.24 \pm 0.14$	$-0.52 \pm 0.06$	$-1.05 \pm 0.21$
NGC 7793	$-0.69 \pm 0.13$	$+0.43 \pm 0.13$	$-1.17 \pm 0.10$	$-4.42 \pm 0.19$	$-2.13 \pm 0.18$	$+1.60 \pm 0.16$	$-2.29 \pm 0.26$
UGC 9560	$-1.99 \pm 0.06$	$-1.74 \pm 0.05$	$-1.54 \pm 0.07$	$-1.27 \pm 0.12$	$-2.51 \pm 0.13$	$-0.20 \pm 0.08$	$+1.24 \pm 0.18$

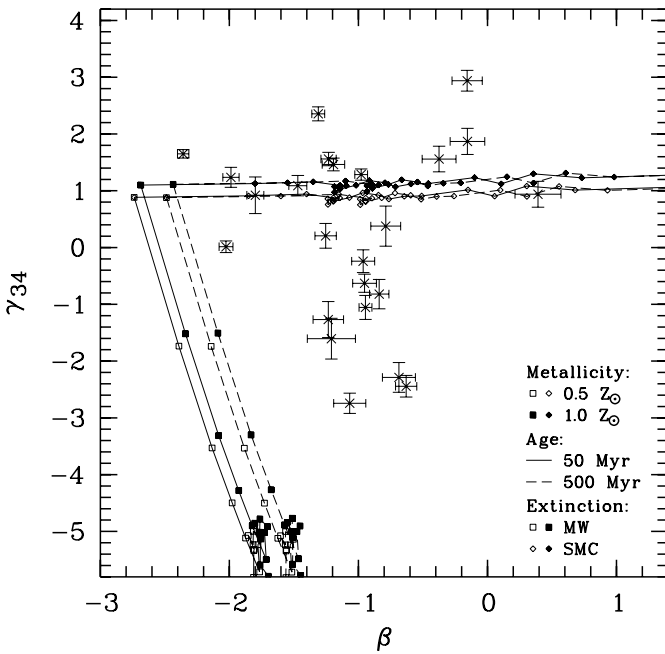


**Fig. 8.** The combined slope parameter  $\gamma_{34}$  versus  $\beta$  for the IUE sample of local starburst galaxies. The statistical uncertainties of the slope measurements are indicated by error bars. For  $\gamma_{34}$  these are probably smaller than the systematic uncertainties (see Sect. 2.2). The spectroscopic data are compared to combined M05 stellar population synthesis and WG00 radiative transfer models. All M05 models shown (see legend) were calculated for a standard Salpeter IMF and continuous star-formation. All WG00 models given (see legend) were calculated for a clumpy SHELL dust/stars configuration. The free parameter of the curves is the average radial visual optical depth  $\tau_V$  (see Fig. 4).

the same conclusions of Gordon et al. (1997) and WG00 for the sample of 30 nearby starbursts with IUE data selected by Calzetti et al. (1994). Hence, our method of analysis is proved to be reliable.

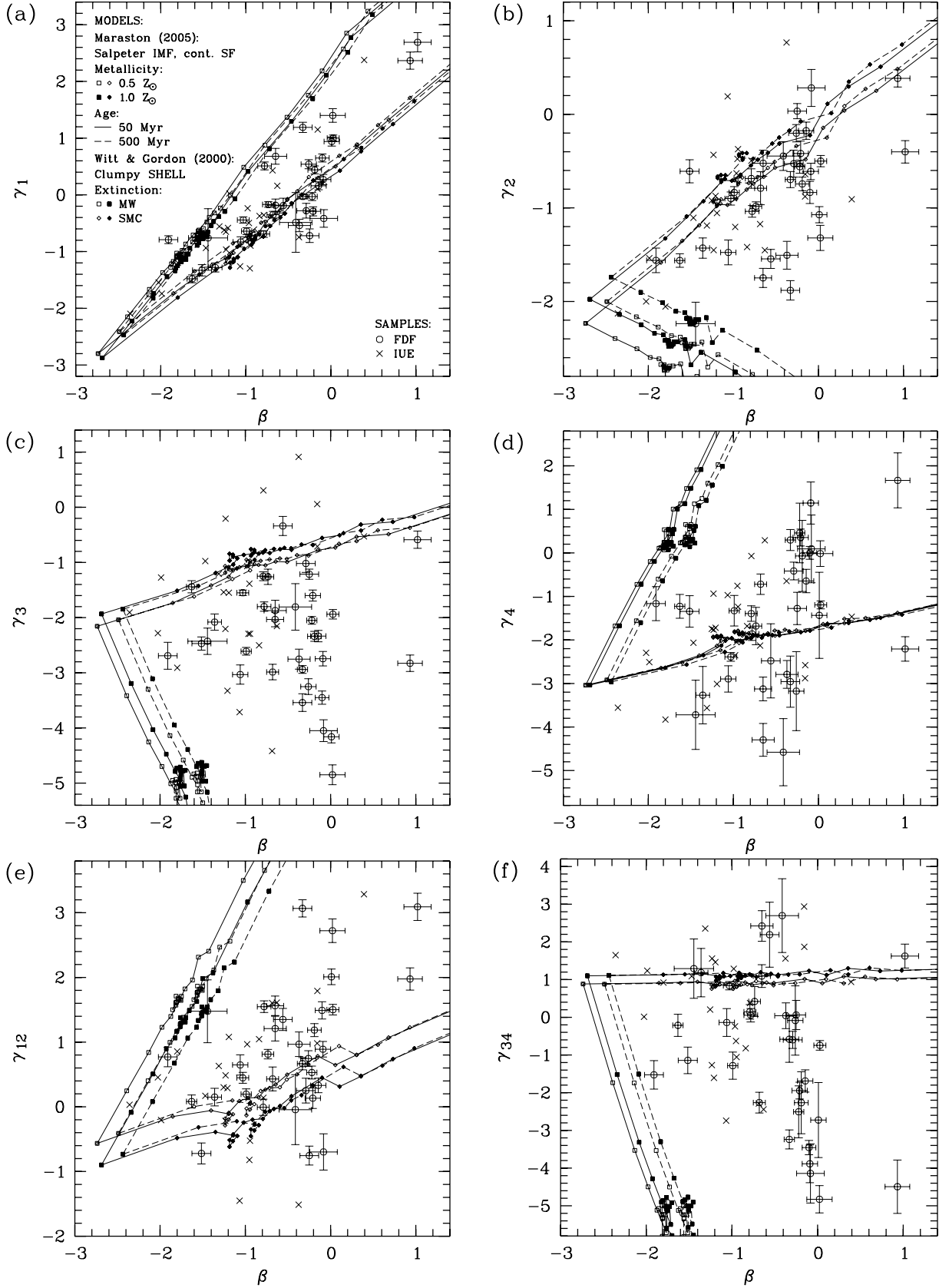
#### 4. Results

Table 7 lists the values of the UV continuum slopes  $\beta$  and  $\gamma_1$  to  $\gamma_4$ , together with the parameters  $\gamma_{12}$  and  $\gamma_{34}$  measured for the FDF sample of 34 UV-luminous galaxies at  $2 < z < 2.5$  (see Sect. 2.1). Hereafter, we will investigate the distribution of these galaxies in diagnostic diagrams defined by  $\beta$  and one of the six  $\gamma$  parameters in comparison with that of the 24 local starbursts of the IUE sample (see Sect. 2.2 and Table 6) and of models combining stellar population synthesis and dust attenuation as in Sect. 3.2.3.

Meurer et al. (1999) proposed the  $\beta$  parameter as a measure of dust attenuation at UV wavelengths for nearby and distant starburst galaxies. More recently, Leitherer et al. (2002) determine

$$A_{1500}[\text{mag}] = 2.19(\beta - \beta_0), \quad \beta_0 = -2.5 \quad (1)$$

as the relation between  $\beta$  and the attenuation at 1500 Å for nearby starburst galaxies. However, radiative transfer modelling (WG00) demonstrates that the “standard”  $\beta$  parameter is a model-dependent measure of dust attenuation at UV wavelengths. In particular, Fig. 4 illustrates the relation between  $\beta$  and  $A_{1500}$  for the WG00 models discussed in Sect. 3.1.2. Furthermore, it shows that  $\beta$  is not a linear measure of dust



**Fig. 9.** The slope parameters  $\gamma_1$  to  $\gamma_4$ ,  $\gamma_{12} = \gamma_1 - \gamma_2$ , and  $\gamma_{34} = \gamma_3 - \gamma_4$  versus  $\beta$  for the FDF sample of  $2 < z < 2.5$  galaxies (open circles with error bars) and the IUE sample of local starburst galaxies (crosses). The spectroscopic data are compared to combined M05 stellar population synthesis and WG00 radiative transfer models. Details of the models shown are indicated in the legend of subfigure a). The free parameter of the curves is the average radial visual optical depth  $\tau_V$  (see Fig. 4).

**Table 7.** UV continuum slope parameters of our sample of 34 FDF galaxies at  $2 < z < 2.5$  (see Table 1).

No.	$\beta$	$\gamma_1$	$\gamma_2$	$\gamma_3$	$\gamma_4$	$\gamma_{12}$	$\gamma_{34}$
1208	$-0.25 \pm 0.11$	$-0.72 \pm 0.12$	$+0.03 \pm 0.08$	$-1.21 \pm 0.09$	$-1.28 \pm 0.37$	$-0.75 \pm 0.15$	$+0.06 \pm 0.39$
1691	$-0.29 \pm 0.11$	$-0.28 \pm 0.13$	$-0.53 \pm 0.14$	$-1.02 \pm 0.16$	$-0.42 \pm 0.20$	$+0.25 \pm 0.19$	$-0.60 \pm 0.23$
1744	$-0.65 \pm 0.13$	$+0.68 \pm 0.14$	$-0.52 \pm 0.14$	$-1.87 \pm 0.19$	$-4.30 \pm 0.38$	$+1.21 \pm 0.19$	$+2.42 \pm 0.41$
1991	$-1.44 \pm 0.23$	$-0.76 \pm 0.52$	$-2.24 \pm 0.23$	$-2.43 \pm 0.24$	$-3.72 \pm 0.79$	$+1.48 \pm 0.49$	$+1.29 \pm 0.79$
2274	$-0.74 \pm 0.07$	$-0.17 \pm 0.05$	$-0.98 \pm 0.05$	$-1.26 \pm 0.14$	$-1.68 \pm 0.43$	$+0.81 \pm 0.07$	$+0.42 \pm 0.40$
2418	$-0.21 \pm 0.09$	$-0.29 \pm 0.08$	$-0.42 \pm 0.13$	$-1.60 \pm 0.10$	$+0.35 \pm 0.19$	$+0.13 \pm 0.16$	$-1.94 \pm 0.22$
2495	$-0.22 \pm 0.06$	$-0.03 \pm 0.07$	$-0.56 \pm 0.07$	$-2.05 \pm 0.07$	$+0.46 \pm 0.69$	$+0.53 \pm 0.10$	$-2.51 \pm 0.69$
2636	$+0.93 \pm 0.14$	$+2.37 \pm 0.15$	$+0.38 \pm 0.09$	$-2.83 \pm 0.15$	$+1.67 \pm 0.63$	$+1.98 \pm 0.17$	$-4.49 \pm 0.71$
3005	$-0.14 \pm 0.09$	$+0.16 \pm 0.07$	$-0.18 \pm 0.09$	$-2.34 \pm 0.10$	$-0.65 \pm 0.27$	$+0.33 \pm 0.11$	$-1.69 \pm 0.29$
3163	$-0.19 \pm 0.08$	$+0.44 \pm 0.07$	$-0.74 \pm 0.07$	$-2.34 \pm 0.09$	$-0.07 \pm 0.82$	$+1.19 \pm 0.10$	$-2.27 \pm 0.82$
3300	$-1.36 \pm 0.08$	$-1.28 \pm 0.08$	$-1.43 \pm 0.11$	$-2.08 \pm 0.15$	$-3.27 \pm 0.66$	$+0.15 \pm 0.14$	$+1.19 \pm 0.64$
3374	$-1.63 \pm 0.06$	$-1.48 \pm 0.07$	$-1.56 \pm 0.07$	$-1.44 \pm 0.11$	$-1.23 \pm 0.27$	$+0.08 \pm 0.10$	$-0.21 \pm 0.29$
3688	$-0.33 \pm 0.11$	$+1.19 \pm 0.09$	$-1.88 \pm 0.10$	$-3.54 \pm 0.16$	$-2.96 \pm 0.59$	$+3.07 \pm 0.13$	$-0.58 \pm 0.61$
3810	$-0.33 \pm 0.06$	$-0.03 \pm 0.04$	$-0.70 \pm 0.09$	$-2.94 \pm 0.07$	$+0.30 \pm 0.24$	$+0.67 \pm 0.09$	$-3.24 \pm 0.25$
3874	$+0.01 \pm 0.09$	$+0.94 \pm 0.08$	$-1.07 \pm 0.09$	$-4.16 \pm 0.11$	$-1.43 \pm 0.99$	$+2.01 \pm 0.12$	$-2.73 \pm 1.00$
3875	$-1.52 \pm 0.11$	$-1.33 \pm 0.10$	$-0.61 \pm 0.12$	$-2.47 \pm 0.12$	$-1.34 \pm 0.36$	$-0.72 \pm 0.16$	$-1.14 \pm 0.35$
3958	$-0.65 \pm 0.10$	$-0.18 \pm 0.11$	$-1.75 \pm 0.10$	$-2.03 \pm 0.13$	$-3.13 \pm 0.27$	$+1.56 \pm 0.15$	$+1.09 \pm 0.30$
4795	$-0.78 \pm 0.08$	$+0.51 \pm 0.07$	$-1.04 \pm 0.06$	$-1.80 \pm 0.08$	$-1.86 \pm 0.15$	$+1.55 \pm 0.09$	$+0.05 \pm 0.18$
4871	$-0.09 \pm 0.09$	$+0.27 \pm 0.09$	$-0.61 \pm 0.09$	$-2.75 \pm 0.13$	$+1.15 \pm 0.48$	$+0.89 \pm 0.12$	$-3.89 \pm 0.50$
4996	$+0.03 \pm 0.07$	$+1.00 \pm 0.05$	$-0.50 \pm 0.06$	$-1.94 \pm 0.09$	$-1.19 \pm 0.09$	$+1.50 \pm 0.08$	$-0.74 \pm 0.13$
5058	$-1.03 \pm 0.07$	$-0.44 \pm 0.05$	$-0.90 \pm 0.07$	$-1.55 \pm 0.05$	$-2.39 \pm 0.10$	$+0.45 \pm 0.08$	$+0.84 \pm 0.11$
5135	$-0.37 \pm 0.13$	$-0.54 \pm 0.11$	$-1.51 \pm 0.15$	$-2.75 \pm 0.18$	$-2.79 \pm 0.32$	$+0.97 \pm 0.19$	$+0.04 \pm 0.34$
5165	$-1.06 \pm 0.09$	$-0.83 \pm 0.09$	$-1.48 \pm 0.13$	$-3.03 \pm 0.17$	$-2.90 \pm 0.30$	$+0.65 \pm 0.16$	$-0.14 \pm 0.37$
5190	$-1.91 \pm 0.11$	$-0.79 \pm 0.07$	$-1.56 \pm 0.13$	$-2.69 \pm 0.24$	$-1.17 \pm 0.39$	$+0.77 \pm 0.15$	$-1.53 \pm 0.38$
5227	$+0.02 \pm 0.15$	$+1.40 \pm 0.12$	$-1.32 \pm 0.13$	$-4.85 \pm 0.18$	$-0.02 \pm 0.29$	$+2.72 \pm 0.18$	$-4.83 \pm 0.36$
6024	$-0.99 \pm 0.06$	$-0.64 \pm 0.06$	$-0.84 \pm 0.06$	$-2.61 \pm 0.07$	$-1.33 \pm 0.35$	$+0.20 \pm 0.08$	$-1.28 \pm 0.36$
6372	$-0.79 \pm 0.07$	$-0.69 \pm 0.06$	$-0.69 \pm 0.10$	$-1.25 \pm 0.08$	$-1.39 \pm 0.18$	$-0.01 \pm 0.13$	$+0.14 \pm 0.19$
6407	$+1.02 \pm 0.16$	$+2.69 \pm 0.17$	$-0.40 \pm 0.12$	$-0.59 \pm 0.16$	$-2.21 \pm 0.28$	$+3.09 \pm 0.21$	$+1.62 \pm 0.32$
6934	$-0.26 \pm 0.09$	$+0.54 \pm 0.08$	$-0.20 \pm 0.09$	$-3.25 \pm 0.14$	$-3.18 \pm 0.91$	$+0.75 \pm 0.12$	$-0.09 \pm 0.92$
6947	$-0.10 \pm 0.08$	$+0.65 \pm 0.07$	$-0.84 \pm 0.12$	$-3.45 \pm 0.12$	$+0.00 \pm 0.15$	$+1.49 \pm 0.13$	$-3.46 \pm 0.19$
7029	$-0.68 \pm 0.07$	$-0.35 \pm 0.06$	$-0.79 \pm 0.18$	$-2.99 \pm 0.14$	$-0.72 \pm 0.23$	$+0.43 \pm 0.18$	$-2.26 \pm 0.27$
7078	$-0.41 \pm 0.19$	$-0.49 \pm 0.53$	$-0.45 \pm 0.15$	$-1.81 \pm 0.42$	$-4.58 \pm 0.77$	$-0.04 \pm 0.54$	$+2.70 \pm 0.98$
7307	$-0.56 \pm 0.11$	$-0.19 \pm 0.13$	$-1.55 \pm 0.10$	$-0.34 \pm 0.17$	$-2.48 \pm 0.85$	$+1.35 \pm 0.17$	$+2.19 \pm 0.86$
7342	$-0.08 \pm 0.16$	$-0.42 \pm 0.15$	$+0.28 \pm 0.20$	$-4.05 \pm 0.20$	$+0.09 \pm 0.78$	$-0.70 \pm 0.28$	$-4.14 \pm 0.79$

**Table 8.** Average UV continuum slope parameters of the local IUE sample and different  $2 < z < 2.5$  FDF samples. The slope parameters were averaged unweighted. The uncertainties given are mean errors and were derived from the variance of the sample without considering the individual errors.

Par.	IUE	FDF	FDF	FDF	FDF	FDF
	all	all	$\beta < -0.4$	$-0.4 < \beta < 0.1$	$-0.4 < \beta < 0.1$	$\gamma_{34} > -2$
$N$	24	34	16	16	8	8
$\beta$	$-1.05 \pm 0.13$	$-0.50 \pm 0.11$	$-1.01 \pm 0.11$	$-0.18 \pm 0.03$	$-0.23 \pm 0.04$	$-0.12 \pm 0.04$
$\gamma_1$	$-0.51 \pm 0.16$	$+0.03 \pm 0.16$	$-0.53 \pm 0.15$	$+0.27 \pm 0.16$	$+0.13 \pm 0.25$	$+0.40 \pm 0.21$
$\gamma_2$	$-0.98 \pm 0.14$	$-0.86 \pm 0.11$	$-1.15 \pm 0.13$	$-0.67 \pm 0.14$	$-0.65 \pm 0.24$	$-0.69 \pm 0.17$
$\gamma_3$	$-1.63 \pm 0.26$	$-2.33 \pm 0.17$	$-1.98 \pm 0.18$	$-2.76 \pm 0.27$	$-2.21 \pm 0.33$	$-3.32 \pm 0.34$
$\gamma_4$	$-1.90 \pm 0.22$	$-1.46 \pm 0.26$	$-2.34 \pm 0.30$	$-0.73 \pm 0.33$	$-1.51 \pm 0.46$	$+0.06 \pm 0.26$
$\gamma_{12}$	$+0.46 \pm 0.21$	$+0.88 \pm 0.17$	$+0.62 \pm 0.17$	$+0.94 \pm 0.27$	$+0.78 \pm 0.40$	$+1.10 \pm 0.36$
$\gamma_{34}$	$+0.27 \pm 0.32$	$-0.87 \pm 0.35$	$+0.36 \pm 0.36$	$-2.04 \pm 0.40$	$-0.69 \pm 0.27$	$-3.38 \pm 0.31$

attenuation at UV wavelengths along the whole range potentially available for  $A_{1500}$  for a sample of objects, even when dust attenuation can be described in the same way for all these objects. With these caveats in mind, we determine the mean value of  $\beta$  to be  $\langle \beta \rangle = -1.05 \pm 0.13$  for the IUE sample and  $\langle \beta \rangle = -0.50 \pm 0.11$  for the FDF sample (see Table 8). If the

stellar populations, the dust/stars configuration, and the structure of the dusty ISM are the same for the galaxies of both samples (see Sect. 3.1), then Fig. 4 implies that the mean attenuation at UV wavelengths is larger for the FDF galaxies (see also Noll et al. 2004). In this case, we probably compare  $z \sim 2$  ultraluminous galaxies (i.e. with  $L_{\text{UV}} \gtrsim 10^{12} L_{\odot}$ ) to fainter

(by about two orders of magnitude) local starburst galaxies (see Heckman et al. 1998; Leitherer et al. 2002), given the gap in observed UV luminosities (see Fig. 1).

Figure 9 shows the distribution of the FDF and IUE sample galaxies and the loci of the models in several diagrams where the individual  $\gamma$  parameters are plotted versus  $\beta$ . Open circles and crosses reproduce, respectively, the  $z \sim 2$  UV-luminous FDF galaxies and the local IUE starbursts. For both samples, the measured parameters have similar uncertainties, though for the FDF sample the most uncertain one is  $\gamma_4$  due to the bright night sky in the corresponding wavelength range. For the IUE sample the uncertainties of  $\gamma_3$  are particularly high due to the low quality of the combined spectra in the overlapping region of the IUE short and long wavelength channels (see Sect. 2.2). Therefore, only error bars for the FDF galaxies are drawn to ease the reading of Fig. 9. Different models are reproduced synthetically as illustrated in Fig. 9a. We discuss the results obtained from the analysis of Fig. 9 in the next two sections.

#### 4.1. The far-UV slope of the extinction law

Panels a, b, and e of Fig. 9 show, respectively,  $\gamma_1$ ,  $\gamma_2$ , and  $\gamma_{12}$  versus  $\beta$  both for the observed spectra and the synthetic ones. As the models show, the distribution in these three diagrams characterises the far-UV slope of the extinction law. Not surprisingly, both the models and the observed galaxies are distributed almost along the one-to-one relation in the  $\beta - \gamma_1$  plane. This is due to the large overlap between the wavelength windows where the two slopes are defined (see Fig. 5). Models with different extinction curves split up much better in the  $\beta - \gamma_2$  and  $\beta - \gamma_{12}$  planes. In fact,  $\gamma_2$  and  $\beta$  are defined in wavelength regions with only a partial overlap.

Interestingly, most of the FDF and IUE galaxies are distributed in the region delimited by the models with MW or SMC dust in each diagram. However, the baricenter of the galaxy distribution is close to the locus of the models with SMC extinction law, despite the scatter of the distribution is large. We conclude that the mixture of dust grains present in the UV-luminous FDF galaxies at  $z \sim 2$  produces an extinction curve with a far-UV slope that is intermediate between those of the MW and SMC extinction curves, if not close to the far-UV slope of the SMC extinction curve.

This result is robust against differences in the stellar populations induced by metallicity, age, and star-formation history of the real galaxies, for the reasons discussed in Sect. 3.2.2. Small differences do exist between the distributions of models and galaxies reproduced in panels a, b, and e of Fig. 9 however. For instance,  $\gamma_1$  is sensitive to the maximum age of the stellar populations (i.e. the age of the model), while  $\gamma_2$  is sensitive to the metallicity of the stellar populations (see Table 5). Therefore, individual galaxies will shift slightly with respect to the loci of models with different dust types in the  $\beta - \gamma_1$ ,  $\beta - \gamma_2$ , and  $\beta - \gamma_{12}$  planes according to the true characteristic age and metallicity of their stellar populations.

Furthermore, we note that 26 of 34 UV-luminous FDF galaxies at  $z \sim 2$  exhibit  $\beta > -0.8$ , which can be achieved

by the two-phase, clumpy SHELL models with SMC dust for  $\tau_V > 3-5$ , depending on the properties of the stellar population. In this case the dusty clumps are optically thick at UV wavelengths, and the UV photons escaping from the system do so after scattering through the diffuse interclump medium that is still optically thin (see Sect. 3.1.2). The values of the optical depths of a typical clump and of the diffuse interclump medium depend on the filling factor and density contrast assumed, once  $\tau_V$  is fixed (see Witt & Gordon 1996, WG00). Nevertheless, multiple scattering does play a role in the escape of the UV photons from the reddest, dustiest galaxies of the FDF sample under study.

#### 4.2. Evidence for the presence of the UV bump

Panels c, d, and f of Fig. 9 show, respectively,  $\gamma_3$ ,  $\gamma_4$ , and  $\gamma_{34}$  versus  $\beta$  both for the observed spectra and the synthetic ones. The parameters  $\gamma_3$  and  $\gamma_4$  are defined in wavelength windows corresponding to, respectively, the blue and red wings of the 2175 Å feature present in the average MW and LMC extinction curves. As the models show, the parameters  $\gamma_3$  and  $\gamma_{34}$  are the most sensitive to the presence of the carriers of the UV bump as determined from an observed spectrum. Furthermore, we recall that  $\gamma_3$  and  $\gamma_4$  are affected by relatively large errors for, respectively, the IUE and FDF samples.

Now, Figs. 9c and f clearly show that the  $z \sim 2$  UV-luminous FDF galaxies populate a region delimited by models with either a MW- or an SMC-type extinction curve. Furthermore, Fig. 9f suggests that  $\gamma_{34}$  becomes more negative when  $\beta$  increases. This trend means that the 2175 Å feature characterises the redder, i.e. more attenuated and dustier, FDF galaxies. Conversely, the IUE nearby starbursts are almost equally distributed across the locus of models with SMC-type dust.

These findings are consistent with those illustrated in the previous section, based on  $\gamma$  parameters defined in distinct windows corresponding to the short-wavelength region of the UV spectral domain. Hence, we conclude that the redder, UV-luminous FDF galaxies at  $2 < z < 2.5$  contain a mixture of dust grains producing an extinction curve that has both a far-UV slope and a strength of the UV bump that are intermediate between those of the SMC- and MW-type extinction curves.

#### 4.3. Different dust properties for different galaxy subsamples

Almost all the nearby IUE starbursts exhibit  $\beta < -0.4$ , the mean value of this parameter being  $\langle \beta \rangle = -1.05 \pm 0.13$  (see Table 8). For this reference sample,  $\langle \gamma_{34} \rangle = +0.27 \pm 0.32$ , i.e. the evidence for the presence of the UV bump is weak.

Hence, we divide the  $z \sim 2$  UV-luminous FDF galaxies in two subsamples, with either  $\beta < -0.4$  or  $-0.4 < \beta < 0.1$ . We find that the FDF subsample of 16 objects with  $\beta < -0.4$  exhibits  $\langle \beta \rangle = -1.01 \pm 0.11$  and  $\langle \gamma_{34} \rangle = +0.36 \pm 0.36$ , in good agreement with the reference sample at  $z \sim 0$ . Conversely, the FDF subsample of 16 objects with  $-0.4 < \beta < 0.1$  exhibits  $\langle \beta \rangle = -0.18 \pm 0.03$  and  $\langle \gamma_{34} \rangle = -2.04 \pm 0.40$ . This

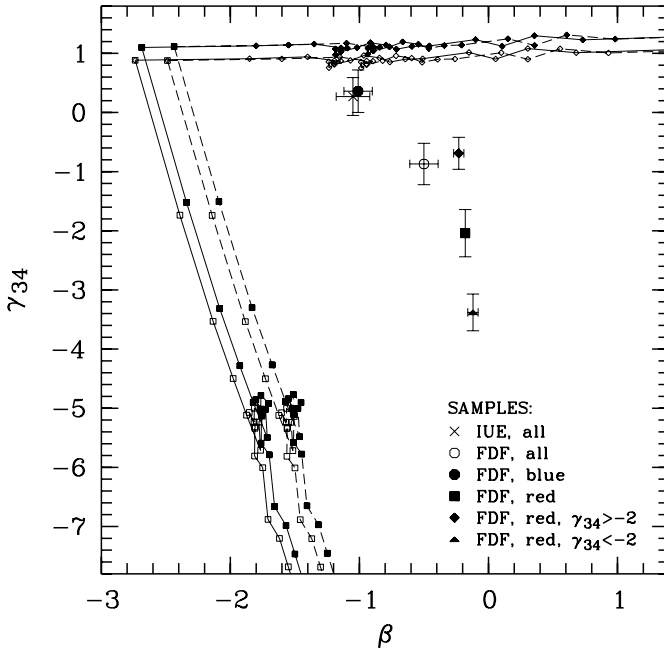


**Fig. 10.** The UV-bump indicator  $\gamma_{34}$  as a function of the reddening measure  $\beta$  for our local galaxy sample (cross) and different subsamples of  $2 < z < 2.5$  FDF galaxies. The complete FDF sample of 34 galaxies (open circle) was divided into a blue ( $\beta < -0.4$ ; 16 objects; filled circle) and a red subsample ( $-0.4 < \beta < 0.1$ ; 16 objects; filled square) excluding two very red objects with  $\beta \sim 1$ . Moreover, the red sample was further fragmented into two subsamples of eight objects each differing in  $\gamma_{34}$ . The filled lozenge and the filled triangle mark galaxies with  $\gamma_{34} > -2$  and  $\gamma_{34} < -2$ , respectively. The  $1\sigma$  error bars indicate mean errors. The diagram also shows combined stellar population synthesis and radiative transfer models as a function of the optical depth of the dust. Details of the models shown are indicated in the legend of Fig. 9a.

confirms that the carriers of the  $2175 \text{ \AA}$  dust absorption feature are present in red (i.e. with  $\beta > -0.4$ ) UV-luminous FDF galaxies at  $z \sim 2$ . Nevertheless, objects with MW-type dust seem not to be present among the FDF sample galaxies as well as in the IUE sample.

The presence of the UV bump can be appreciated directly from the composite spectrum of the eight FDF galaxies with  $\beta > -0.4$  and  $\gamma_{34} < -2$  ( $\langle \gamma_{34} \rangle = -3.4$ ), reproduced in Fig. 11. As a reference, the composite spectrum of the 16 FDF galaxies with  $\beta < -0.4$  ( $\langle \gamma_{34} \rangle = 0.4$ ) is also shown. The two spectra are normalised in the wavelength range from  $1250$  to  $1500 \text{ \AA}$ . The ratio between the “blue” and “red” composite spectra exhibits a broad feature centred at  $2166 \pm 15 \text{ \AA}$ , consistent with the centre of the UV bump. Its slope is negative owing to the different values of  $\beta$  for the two subsamples.

Having established the presence of a UV bump in the extinction curves of the red UV-luminous FDF galaxies at  $z \sim 2$ , can we also estimate its strength? Unfortunately, there are no WG00 models for extinction curves different from those typical either of the diffuse ISM of the Milky Way or of the SMC bar. Therefore, for illustrational purposes only, we show the distribution in the  $\beta - \gamma_{34}$  plane of models where dust attenuation is described by a non-scattering homogeneous dust screen

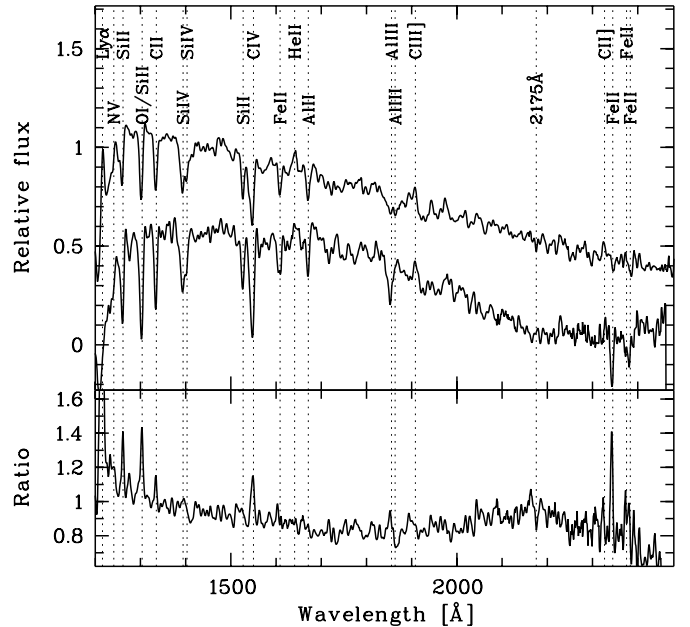


**Fig. 11.** Comparison of composite spectra of FDF galaxies in the range  $2.0 < z < 2.5$  differing in  $\beta$  and  $\gamma_{34}$ . Upper spectrum in the *upper panel*: composite of 16 FDF galaxies with  $\beta < -0.4$ . Lower spectrum in the upper panel (offset by  $-0.5$  for clarity): composite of eight FDF galaxies with  $-0.4 < \beta < 0.1$  and  $\gamma_{34} < -2$ . The *lower panel* gives the ratio of both composites. The positions of prominent UV lines and the UV dust feature are indicated.

for different empirical extinction laws as a function of  $E_{B-V}$  (see Calzetti et al. 2000; Gordon et al. 2003). In particular, we consider the extinction functions determined for the SMC bar, the LMC 2 supershell region, the average LMC (Gordon et al. 2003), and the average MW (CCM), that are displayed in Fig. 3. As a reference, we take the attenuation functions produced by the two-phase, clumpy SHELL models with MW- or SMC-type dust of WG00, and the Calzetti et al. (2000) attenuation law. This comparison holds only to the purpose of comparing slopes of synthetic spectra (see Sect. 3.1.2). Figure 12 reproduces the loci of the different models and the distribution of the FDF and IUE sample galaxies. It is evident that a mixture of dust grains with properties ranging from those typical of the SMC bar to those typical of the LMC 2 supershell region can account for the distribution of the data in the  $\beta - \gamma_{34}$  plane. We recall that the LMC 2 supershell region is located near the extremely vigorous 30 Dor star-formation region (Misselt et al. 1999). Conversely, extinction curves typical of more quiescent star-formation activities like those of the average LMC and MW seem not to describe the distribution of the data in the previous plane. This is consistent with the nature of actively star-forming galaxies of the FDF and IUE sample galaxies (see Sect. 2.3).

Comparing the  $\gamma_{12}$  values for the different subsamples defined above (see Table 8), we do not find a significant relation between the far-UV slopes of the extinction function as indicated by  $\gamma_{12}$  and the bump strength. The moderate increase of  $\gamma_{12}$  with  $\beta$  is consistent with the predictions from the WG00 models for SMC-type dust, for which the mean values are in better agreement than for the MW-type models (see Sect. 4.1).

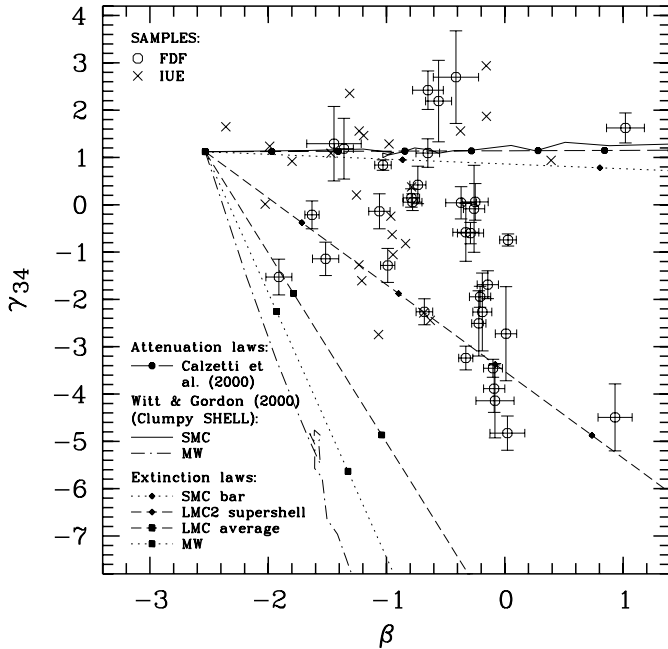


**Fig. 12.** The UV-bump indicator  $\gamma_{34}$  as a function of the reddening measure  $\beta$  for our local (crosses) and  $2 < z < 2.5$  FDF galaxies (circles). The diagram also shows combined stellar population synthesis and dust attenuation models as a function of the optical depth of the dust. The dust attenuation models plotted are the Calzetti et al. (2000) law (long dashed lines and circles) and the WG00 models for the clumpy SHELL configuration with SMC (solid lines) and MW dust (dash-dotted lines). Furthermore, the extinction laws of the SMC bar (dotted lines and lozenges), the LMC2 supershell (dashed lines and lozenges), the LMC average (dashed lines and squares), and the MW (dotted lines and squares) are indicated (CCM; Gordon et al. 2003). The symbols are plotted in intervals of  $\Delta E_{B-V} = 0.1$ . In all cases a M05 model with Salpeter IMF, continuous star-formation, an age of 200 Myr, and solar metallicity has been taken.

#### 4.4. Presence of the UV bump and strengths of stellar and interstellar lines

Hereafter we investigate whether the presence of the UV bump is linked either to the (stellar) metallicity or to properties of the ISM of the system, as traced by the equivalent widths of the absorption lines listed in Table 3. We group the objects in subsamples, as in Sect. 4.3.

Figure 13 reproduces  $\gamma_{34}$  versus  $W_{\text{CIV}}$ .  $W_{\text{CIV}}$  is a good metallicity indicator in starburst galaxies, the CIV feature being mainly produced by hot star winds with a strength that depends on the chemical composition (Walborn et al. 1995; Heckman et al. 1998; Leitherer et al. 2001; Mehlert et al. 2002). Interestingly,  $W_{\text{CIV}}$  is smaller for the subsample of blue UV-luminous FDF galaxies at  $z \sim 2$ , as well as for the IUE sample of nearby starbursts, than for the red subsample of FDF galaxies. However, red FDF galaxies selected according to their values of  $\gamma_{34}$  do not exhibit significant differences in  $W_{\text{CIV}}$ . Hence, the metallicity of the OB stars (and, thus, of the ISM where these stars originated) does not primarily determine the presence of the carrier of the 2175 Å dust absorption feature among the  $z \sim 2$  UV-luminous FDF galaxies. This is consistent with studies of extinction curves in the local universe (see

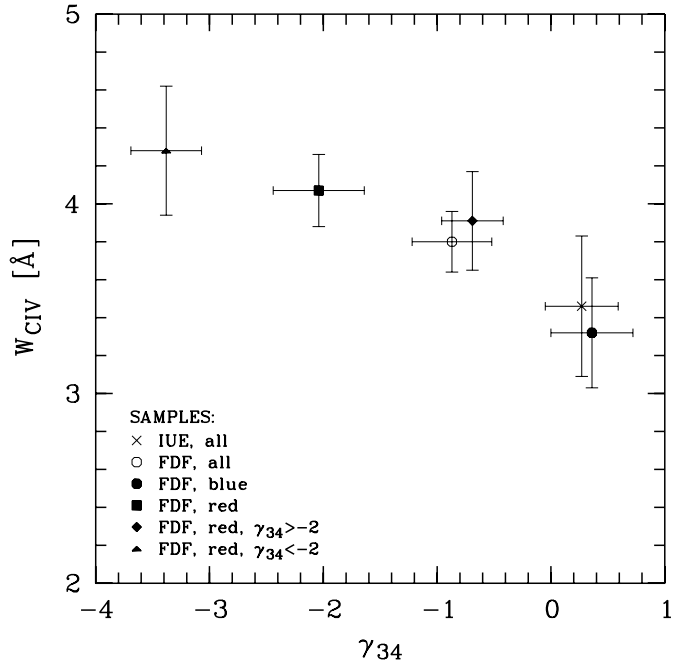


**Fig. 13.** The EW of the metallicity indicator C IV as a function of the UV-bump strength indicator  $\gamma_{34}$  for our local galaxy sample and different subsamples of  $2 < z < 2.5$  FDF galaxies (see legend and caption of Fig. 10). The EWs of C IV were derived from composite spectra of the different samples. The  $1\sigma$  error bars include the variance between the individual spectra, the errors of the continuum level definition, and the statistical uncertainties of the line strengths.

Sect. 1). On the other hand, metallicity is higher (by more than  $2\sigma$ ) for FDF objects affected by a larger reddening at rest-frame UV wavelengths (i.e. with a larger  $\beta$ ). This result holds for the whole FDF spectroscopic sample (Noll et al. 2004).

Finally, the parameter  $\gamma_{34}$  seems to depend also on the average EW of the six most prominent low-ionisation absorption lines that fall within the rest-frame UV domain mapped by FORS ( $W_{\text{LIS}}$ , see Fig. 14). In particular, values of  $\gamma_{34}$  close to zero are associated with low values of  $W_{\text{LIS}}$ . They characterise the IUE local starbursts and the blue  $z \sim 2$  UV-luminous FDF galaxies. On average, the red  $z \sim 2$  UV-luminous FDF galaxies exhibit larger values of  $W_{\text{LIS}}$  (by more than  $1.5\sigma$ ). This difference is essentially caused by the red FDF objects with  $\gamma_{34} < -2$ , having larger values of  $W_{\text{LIS}}$  at almost the  $3\sigma$  level.

This behaviour can be interpreted as follows. The low-ionisation absorption lines trace the spatial and velocity distribution of the neutral interstellar gas illuminated by the rest-frame UV continuum along the observer's line of sight. In particular,  $W_{\text{LIS}}$  is a proxy for the neutral clouds' covering fraction (Shapley et al. 2003). Larger values of  $W_{\text{LIS}}$  imply a larger obscuration at rest-frame UV wavelengths, if the spatial distributions of neutral gas and dust are correlated. Hence, they imply more negative values of  $\gamma_{34}$ , if the extinction curve exhibits a UV bump, as shown by Fig. 10 for the dusty media modelled by WG00.

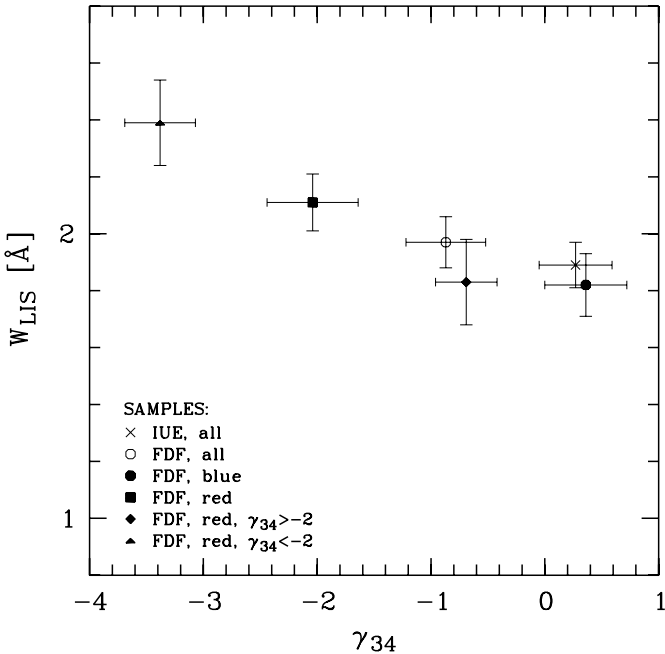


**Fig. 14.** The average strength of six prominent interstellar low-ionisation absorption lines (see Noll et al. 2004) as a function of the UV-bump strength indicator  $\gamma_{34}$  for our local galaxy sample and different subsamples of  $2 < z < 2.5$  FDF galaxies (see legend and caption of Fig. 10). The EWs of the low-ionisation lines were derived in the same way as reported in Fig. 13 for CIV.

## 5. Discussion

Dust grains play a fundamental role in the formation and evolution of galaxies. In fact, they are both a byproduct of stellar evolution (in particular, a sink of metals in the gas phase), as well as a site for the efficient formation of H<sub>2</sub> molecules (e.g. Cazaux & Tielens 2002, 2004). Furthermore, dust grains absorb stellar light and re-emit it at mid-IR-mm wavelengths, controlling the energy balance in the ISM and protostellar gas clouds on one hand, and complicating the interpretation of observed SEDs of any dusty system on the other. Finally, they can offer the surface that is needed for momentum-driven winds on both stellar and galactic scales. Those effects of dust already seem to take place when the metallicity of the environment is very low (i.e.  $\sim 0.01 Z_\odot$ , Hirashita & Ferrara 2002; Morgan & Edmunds 2003). For all those reasons, the first dust enrichment in the course of galaxy evolution may drive an enhanced, high star-formation rate, shaping the cosmic SFR history at the highest redshifts.

The first source of dust in the universe is type II supernovae or pair instability supernovae, beginning to occur a few Myr after the onset of star-formation. After a few  $10^2$  Myr evolved intermediate/low mass stars start to contribute to the dust enrichment. Hence, for the individual galaxy, the relative importance of the two sources of dust depends on time and SFR history (see, e.g., Dwek 1998).

The extinction curves expected in young (i.e. less than 1 Gyr old) galaxies are quite sensitive to internal metal mixing in supernovae (Hirashita et al. 2005). In general, these extinction curves do not exhibit a 2175 Å absorption feature

(as the standard MW extinction curve instead) because the contribution of carbon grains is small (for dust yields, see Todini & Ferrara 2001; Nozawa et al. 2003; Schneider et al. 2004). Furthermore, they are different from the MW, LMC, and SMC extinction curves, especially at rest-frame UV wavelengths (Hirashita et al. 2005). This is no surprise, since the ages of the MW, LMC, and SMC are much longer than 1 Gyr and, thus, at least a change in the dust production mechanism has taken place. Furthermore, the dusty gas outflows of intermediate/low mass stars are carbon rich.

At present, there are only few observational studies on the extinction curves in systems at very high redshift. The extinction properties of broad absorption line quasars at  $z > 4.9$  seem to be different from those of analogous objects at  $z < 4$  (Maiolino et al. 2004a). In particular, the extinction curve of SDSS J1048+4637 at  $z = 6.2$  has been shown to be fitted by dust models of type II supernovae rather than those of pair instability supernovae (Maiolino et al. 2004b). For ages of the universe much longer than 1 Gyr (i.e. for  $z \ll 5$ ), the known extinction curves provide controversial conclusions as for the presence of the 2175 Å absorption feature (see Sect. 1). This may be a consequence of at least a difference in the “characteristic” SFR history of different classes of objects.

In particular, the absence of a pronounced UV bump seems to characterise the average extinction curve in the large, well studied photometric sample of LBGs at  $z \sim 3$  observed by Steidel et al. (2003) (Vijh et al. 2003). Interestingly, the UV bump is weak if not absent also in starburst galaxies of the local universe, whatever their metallicity (Calzetti et al. 1994; Gordon et al. 1997). Is this so for all UV-luminous galaxies down to  $z = 0$  then?

In order to answer to this question, we have investigated the extinction properties in 34 UV-luminous galaxies at  $2 < z < 2.5$  from the FDF spectroscopic survey (see Sect. 2.1). Using a new parametric description of the rest-frame UV spectra (see Sect. 3.2) we have found that most of the  $z \sim 2$  UV-luminous galaxies are characterised by an extinction curve that is intermediate between those of the SMC and the MW (see Sect. 4). This means that the characteristic extinction curve of these objects exhibits a weaker 2175 Å feature but a steeper far-UV rise with respect to the average extinction curve for the diffuse ISM of the MW.

The bulk of the mixture of dust grains (regarding size and chemical composition) present in all the 34 UV-luminous galaxies at  $2 < z < 2.5$  is different from the mixture of dust grains producing the standard MW extinction curve. This is true especially for those galaxies that have probably a low dust content (and, thus, a low value of  $\beta$  as for our models). On the other hand, SMC-like dust may characterise up to 30% of these galaxies. In conclusion, the bulk properties of dust in  $z \sim 2$  UV-luminous galaxies seem to range between those in the SMC and LMC.

The size of the  $z \sim 2$  UV-luminous galaxy sample allows sub-sampling. In general, the 18 “red” (i.e. with  $\beta > -0.4$ ) UV-luminous galaxies at  $2 < z < 2.5$  exhibit a stronger evidence of the presence of the UV bump. The presence of the UV-bump in the eight UV-luminous galaxies at  $z \sim 2$  with  $-0.4 < \beta < 0.1$  and  $\gamma_{34} < -2$  ( $\langle \gamma_{34} \rangle = -3.4$ ) can be appreciated

directly from the ratio of the “blue” and “red” FDF composite spectra reproduced in Fig. 11. This result is at variance with that obtained for the nearby starburst sample, that appears to be characterised by SMC-like dust whatever  $\beta$ , consistent with Gordon et al. (1997), though it mostly exhibits  $\beta < -0.4$ . Our interpretation of this finding is that the carrier of the 2175 Å feature is more abundant in redder and, thus, dustier objects in the  $z \sim 2$  UV-luminous galaxy sample.

On the other hand,  $z \sim 2$  UV-luminous galaxies with  $\beta \sim 0$  exhibit a large scatter in both the parameters  $\gamma_{12}$  and  $\gamma_{34}$  (see Fig. 12 and Table 8). Now,  $\gamma_{12}$  is particularly sensitive to the far-UV slope of the extinction curve, while  $\gamma_{34}$  is particularly sensitive to the presence (and strength) of the UV bump. We conclude that there is no evidence of a correlation between the strength of the far-UV slope and the strength of the UV bump, for the extinction curves of the FDF galaxies with evidence of the UV bump. This may suggest that different environments (in terms of properties of the ISM and of the general radiation field) and/or different degrees of dust processing characterise different  $z \sim 2$  UV-luminous galaxies, if the lessons derived from the local universe apply to the universe at  $z \sim 2$  (see Sect. 1).

The available data allow us to check the first suggestion. We find that the FDF sample galaxies with  $\beta \sim 0$  are characterised by relatively high metallicities of  $Z \sim 0.5\text{--}1 Z_\odot$  (see Mehrt et al. 2002, 2005). However, the metallicity indicator  $W_{\text{CIV}}$  does not show any significant correlation with  $\gamma_{34}$  (see Fig. 13). Hence, a relatively high metallicity (i.e. close to the solar value) seems to be a prerequisite for the occurrence of the UV bump. However, it does not determine the strength of the 2175 Å feature.

Furthermore, the  $z \sim 2$  UV-luminous galaxies with evidence of a relatively strong UV bump are among the most massive and largest galaxies at this redshift. This is shown in Fig. 15, where we plot the estimated total stellar mass<sup>5</sup> (upper panel) and the rest-frame UV effective radius<sup>6</sup> (lower panel) versus  $\beta$ . Nevertheless, there is no correlation between stellar mass or size of a galaxy and the strength of the UV bump. In conclusion, an extinction curve exhibiting the UV bump is likely to be associated with the most massive, largest, and,

<sup>5</sup> The total stellar mass was estimated by Drory et al. (2005) following Brinchmann & Ellis (2000). In particular, Drory et al. (2005) derived stellar masses after applying a large set of two-component models to the whole FDF photometric data (see Heidt et al. 2003). Each model consisted of a combination of two composite stellar populations, as given by a young (100 Myr) burst with a constant SFR plus an older burst ( $\geq 500$  Myr) with an exponentially declining SFR. Both stellar components were attenuated independently according to the “Calzetti law” (Calzetti et al. 2000).

<sup>6</sup> Effective radii and ellipticities were estimated by Pannella et al. (2005), who determined the morphology of the whole FDF galaxies by applying the publicly available two-dimensional surface brightness profile fitting packages GIM2D (Simard et al. 1999) and GALFIT (Peng et al. 2002) to publicly available Hubble ACS images of the FDF in the  $F814W$  broad-band filter. The effective wavelength of this filter corresponds to rest-frame wavelengths of about 2500 Å at  $z \sim 2$ , as for the sample under investigation.

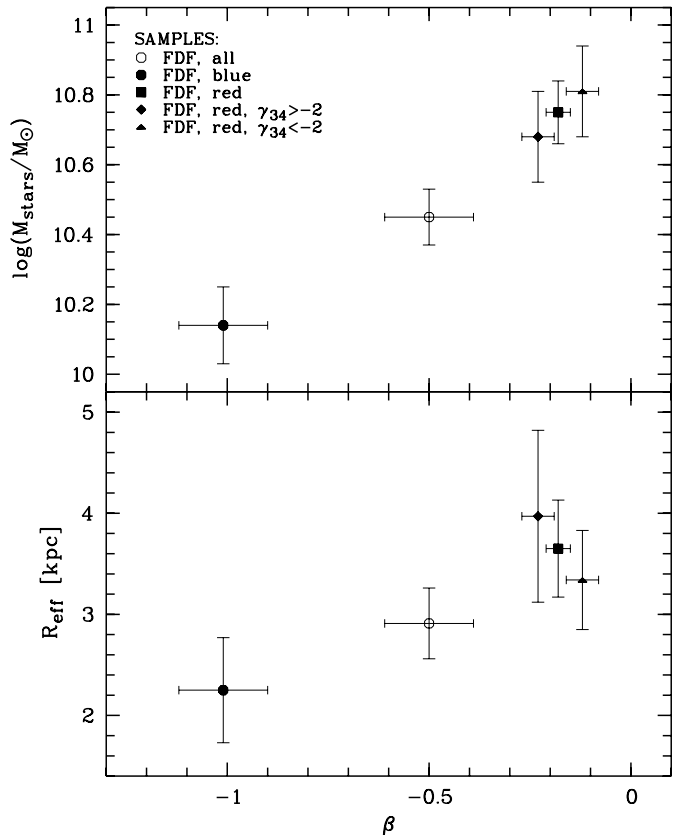


**Fig. 15.** The logarithm of the total stellar mass (Drory et al. 2005) in solar units (upper panel) and the half-light radius (Pannella et al. 2005) in kpc (lower panel) as a function of the reddening measure  $\beta$  for different subsamples of  $2 < z < 2.5$  FDF galaxies (see legend and caption of Fig. 10). The  $1\sigma$  error bars are based on the variance in mass and radius between different galaxies.

possibly, more evolved systems among the  $z \sim 2$  UV-luminous ones.

Finally, we explore the possibility that the topology of the dusty ISM produces the large scatter of  $\gamma_{34}$  observed for the red UV-luminous galaxies at  $2 < z < 2.5$ . This hypothesis is made appealing by the fact that the red UV-luminous galaxies with  $\gamma_{34} < -2$  exhibit a significantly larger  $W_{\text{LIS}}$  than the average  $z \sim 2$  UV-luminous galaxy and the average local starburst galaxy. We recall that  $W_{\text{LIS}}$  traces the covering fraction of the young stellar population by (dusty) neutral gas clouds in the direction to the outside observer. A larger covering fraction may be due to inclination effects, for a disk geometry (e.g. Pierini et al. 2004). For the  $z \sim 2$  FDF objects with  $-0.4 < \beta < 0.1$  we find small but insignificant differences in the average ellipticities  $\epsilon$ <sup>7</sup> for the  $\gamma_{34} > -2$  and  $\gamma_{34} < -2$  subsamples (see Table 8), indicating  $\langle \epsilon \rangle = 0.41 \pm 0.07$  and  $0.55 \pm 0.08$ , respectively. Hence, larger values of  $W_{\text{LIS}}$  possibly imply a better self-shielding of the dust grains that populate the intervening gas clouds, despite inclination effects may be not negligible. The carriers of the 2175 Å feature would then be protected from strong and hard radiation fields by a screen of other (more

<sup>7</sup>  $\epsilon = \sqrt{1 - b^2/a^2}$ ,  $a$  = major axis,  $b$  = minor axis; for the origin of the data see Pannella et al. (2005) and footnote 6.

robust) dust grains (e.g. Gordon et al. 2003). In this case, light emitted by young stars and scattered by the embedding dusty gas clouds plus light emitted by stars living in relatively quiescent environments (e.g. the diffuse ISM) would dominate the UV spectra. On the other hand, smaller values of  $W_{\text{LIS}}$  may imply a larger dust-clearing effect by superwinds (e.g. Strickland & Stevens 2000) in the direction to the outside observer. The effect of superwinds is probably larger in less evolved systems. In this case, the UV spectra would be dominated by light produced in star-formation regions, characterised by strong radiation fields and shocks. In these harsh environments, probably the carriers of the 2175 Å feature would have a larger probability to be destroyed, if ever produced. However, the local universe shows that the latter conclusion is not so straightforward (see Sect. 1).

## 6. Conclusions

We have investigated the properties of the extinction curve in the rest-frame UV for a sample of 34 UV-luminous galaxies at redshift  $2 < z < 2.5$  selected from the FORS Deep Field spectroscopic survey (Noll et al. 2004). Our analysis makes use of a new parametric description of the rest-frame UV spectra of the observed objects and of synthetic spectra. The latter spectra are computed with models combining stellar population evolutionary synthesis (Maraston 2005, M05) and radiative transfer of the stellar and scattered radiation through different dusty interstellar media for the SHELL dust/stars configuration, in a spherically symmetric geometry (Witt & Gordon 2000, WG00).

Firstly, we have established how much the new parameters (seven in total) depend on the properties of the stellar populations or of dust attenuation assumed for galaxy models aimed at reproducing the rest-frame UV spectra of star-forming galaxies.

Secondly, the robustness of our method has been tested against a reference sample of 24 nearby starbursts. Comfortably, we reproduce the result that local starburst galaxies possibly contain dust with an extinction curve lacking the 2175 Å absorption feature (or “UV bump”), like the Small Magellanic Cloud (SMC) but at variance with the Milky Way (MW), and a steep far-UV rise, intermediate between those in the SMC and the MW extinction curves (Calzetti et al. 1994; Gordon et al. 1997).

The application of the same method to the sample of  $z \sim 2$  UV-luminous galaxies leads to the following results.

- The UV-luminous galaxies at  $2 < z < 2.5$  with a relatively low amount of reddening at rest-frame UV wavelengths (i.e. with a far-UV slope  $\beta < -0.4$ ) contain a mixture of dust grains that is similar to that held to be present in local starburst galaxies. This analogy holds despite the fact that the former galaxies are about one order of magnitude more luminous than the latter.
- For the highly reddened (i.e. with  $-0.4 < \beta < 0.1$ )  $z \sim 2$  UV-luminous galaxies, the extinction curves range between those typical of the SMC and Large Magellanic Cloud

(LMC). Therefore, part of these objects exhibits UV bumps as pronounced as in the LMC.

- The amount of reddening at rest-frame UV wavelengths is larger in more metal-rich objects, the equivalent width of the CIV doublet ( $W_{\text{CIV}}$ ) being used as an indicator of the total metallicity. On the other hand, objects with large values of  $W_{\text{CIV}}$  (i.e. metal rich) can exhibit both SMC- and LMC-type dust, despite the 2175 Å absorption feature is associated with the presence of carbonaceous dust grains.
- The presence of the UV bump seems to be associated with a large average equivalent width of the six most prominent, rest-frame UV, low-ionisation absorption lines falling in the FORS spectra. The average equivalent width of these saturated lines offers a proxy for the covering fraction of young massive stars by neutral gas clouds (containing dust grains), and, thus, for the ISM topology.
- Furthermore, we find that the most opaque and, thus (for our models), dustiest UV-luminous FDF galaxies at  $z \sim 2$  tend to be among the most metal rich (i.e. with an average metallicity  $\langle Z \rangle \sim 0.5\text{--}1 Z_{\odot}$ ), most massive (i.e. with an average stellar mass  $\langle M_{\text{stars}} \rangle \sim 6 \times 10^{10} M_{\odot}$ ), and largest (i.e. with an average rest-frame UV effective radius  $\langle R_{\text{eff}} \rangle \sim 4 \text{ kpc}$ ) systems.

We interpret these results as the evidence for a difference in the properties of the dusty ISM among the most evolved UV-luminous, massive galaxies at  $z \sim 2$ . As for the local universe, the diversity in the bulk properties of the dust grains from one galaxy to another is possibly caused by the sum of the local effects due to stellar radiation field, shocks, ISM topology, and history of chemical enrichment. In particular, the degree of self-shielding by dust may play an important role for the production and/or survival of the small carbonaceous grains that are held to be the carriers of the UV bump already at  $z \sim 2$ .

**Acknowledgements.** First of all, we thank Claudia Maraston for calculating special composite stellar population synthesis models for our project and for reading the manuscript. Moreover, thanks go to Niv Drory and Maurilio Pannella for providing mass estimates and morphological information for our FDF sample. We thank Karl D. Gordon for a stimulating discussion. We are also grateful to Immo Appenzeller, Ulrich Hopp, Dörte Mehrt, and Christian Tapken for carefully reading the manuscript and for their valuable comments. Finally, we thank the referee for her/his receptive comments. The investigation of our sample of local starburst galaxies has been based on INES data from the IUE satellite and has made use of the NASA/IPAC Extragalactic Database (NED) which is operated by the Jet Propulsion Laboratory, California Institute of Technology, under contract with the National Aeronautics and Space Administration. This research was supported by the German Science Foundation (DFG, SFB 375).

## References

- Bianchi, S., Ferrara, A., & Giovanardi, C. 1996, ApJ, 465, 127  
 Bohlin, R. C., Savage, B. D., & Drake, J. F. 1978, ApJ, 224, 132  
 Brinchmann J., & Ellis, R. S. 2000, ApJ, 536, L77  
 Bruzual, G., & Charlot, S. 2003, MNRAS, 344, 1000 (BC03)  
 Calzetti, D. 1997, AJ, 113, 162  
 Calzetti, D., Kinney, A. L., & Storchi-Bergmann, T. 1994, ApJ, 429, 582

- Calzetti, D., Armus, L., Bohlin, R. C., et al. 2000, ApJ, 533, 682  
 Cardelli, J. A., Clayton, G. C., & Mathis, J. S. 1989, ApJ, 345, 245  
 (CCM)  
 Cazaux, S., & Tielens, A. G. G. M., 2002, ApJ, 575, L29  
 Cazaux, S., & Tielens, A. G. G. M., 2004, ApJ, 604, 222  
 Cimatti, A., Bianchi, S., Ferrara, A., & Giovanardi, C., 1997, MNRAS, 290, L43  
 Clayton, G. C., 2004, in Astrophysics of dust, ed. A. N. Witt, G. C. Clayton, & B. T. Draine, ASP Conf. Ser., 309, 57  
 Clayton, G. C., Gordon, K. D., & Wolff, M. J. 2000, ApJS, 129, 147  
 Daddi, E., Cimatti, A., Renzini, A., et al. 2004, ApJ, 600, L127  
 Désert, F. X., Boulanger, F., & Puget, J. L. 1990, A&A, 237, 215  
 Dopita, M. A., Groves, B. A., Fischer, J., et al. 2005, ApJ, 619, 755  
 Draine, B. T. 2003, ARA&A, 41, 241  
 Draine, B. T., & Li, A. 2001, ApJ, 551, 807  
 Drory, N., Salvato, M., Gabasch, A., et al. 2005, ApJ, 619, L131  
 Dwek, E. 1998, ApJ, 501, 643  
 Dwek, E., Arendt, R. G., Fixsen, D. J., et al., 1997, ApJ, 475, 565  
 Fioc, M., & Rocca-Volmerange, B. 1997, A&A, 326, 950 (FR97)  
 Fischer, J., Dopita, M. A., & Sutherland, R. S. 2003, ApJ, 599, L21  
 Fitzpatrick, E. L. 1999, PASP, 111, 63  
 Fitzpatrick, E. L. 2004, in Astrophysics of dust, ed. A. N. Witt, G. C. Clayton, & B. T. Draine, ASP Conf. Ser., 309, 33  
 Gordon, K. D., Calzetti, D., & Witt, A. N. 1997, ApJ, 487, 625  
 Gordon, K. D., Smith, T. L., & Clayton, G. C. 1999, in The High Redshift Universe: Galaxy Formation and Evolution at High Redshift, ed. A. J. Bunker & W. J. M. van Breugel, ASP Conf. Proc., 193, 517  
 Gordon, K. D., Misselt, K. A., Witt, A. N., & Clayton, G. C., 2001, ApJ, 551, 269  
 Gordon, K. D., Clayton, G. C., Misselt, K. A., Landolt, A. U., & Wolff, M. J. 2003, ApJ, 594, 279  
 Heckman, T. M., Robert, C., Leitherer, C., Garnett, D. R., & van der Rydt, F. 1998, ApJ, 503, 646  
 Heidt, J., Appenzeller, I., Gabasch, A., et al. 2003, A&A, 398, 49  
 Hirashita, H., & Ferrara, A. 2002, MNRAS, 337, 921  
 Hirashita, H., Nozawa, T., Kozasa, T., Ishii, T. T., & Takeuchi, T. T. 2005, MNRAS, 357, 1077  
 Hopkins, P. F., Strauss, M. A., Hall, P. B., et al. 2004, AJ, 128, 1112  
 Inoue, A. K. 2005, MNRAS, 359, 171  
 Johnson, K. E., Vacca, W. D., Leitherer, C., Conti, P. S., & Lipsky, S. J. 1999, AJ, 117, 1708  
 Khare, P., York, D. G., Vanden Berk, D., et al. 2005 [arXiv:astro-ph/0504532]  
 Kinney, A. L., Bohlin, R. C., Calzetti, D., Panagia, N., & Wyse, R. F. G. 1993, ApJS, 86, 5  
 Leitherer, C., Schaerer, D., Goldader, J. D., et al. 1999, ApJS, 123, 3  
 Leitherer, C., Leão, J. R. S., Heckman, T. M., et al. 2001, ApJ, 550, 724  
 Leitherer, C., Li, I.-H., Calzetti, D., & Heckman, T. M. 2002, ApJS, 140, 303  
 Li, A., & Draine, B. T. 2001, ApJ, 554, 778  
 Luck, R. E., & Lambert, D. L. 1992, ApJS, 79, 303  
 Maiolino, R., Marconi, A., Salvati, M., et al. 2001, A&A, 365, 28  
 Maiolino, R., Oliva, E., Ghinassi, F., et al. 2004a, A&A, 420, 889  
 Maiolino, R., Schneider, R., Oliva, E., et al. 2004b, Nature, 431, 533  
 Malhotra, S. 1997, ApJ, 488, L101  
 Maraston, C. 2005, MNRAS, 362, 799 (M05)  
 Mathis, J. S., Rumpl, W., & Nordsieck, K. H. 1977, ApJ, 217, 425  
 Mehrtens, D., Noll, S., Appenzeller, I., et al. 2002, A&A, 393, 809  
 Mehrtens, D., Tapken, C., Appenzeller, I., et al. 2005, in Starbursts, ed. R. de Grijs & R. M. González Delgado (Kluwer), 299  
 Meurer, G. R., Heckman, T. M., & Calzetti, D. 1999, ApJ, 521, 64  
 Misselt, K. A., Clayton, G. C., & Gordon, K. D. 1999, ApJ, 515, 128  
 Misselt, K. A., Gordon, K. D., Clayton, G. C., & Wolff, M. J. 2001, ApJ, 551, 277  
 Morgan, H. L., & Edmunds, M. G. 2003, MNRAS, 343, 427  
 Noll, S., Mehrtens, D., Appenzeller, I., et al. 2004, A&A, 418, 885  
 Nozawa, T., Kozasa, T., Umeda, H., Maeda, K., & Nomoto, K. 2003, ApJ, 598, 785  
 Pannella, M., et al. 2005, in prep.  
 Peng, C. Y., Ho, L. C., Impey, C. D., & Rix, H.-W. 2002, AJ, 124, 266  
 Pierini, D., Gordon, K. D., Witt, A. N., & Madsen, G. J. 2004, ApJ, 617, 1022  
 Pitman, K. M., Clayton, G. C., & Gordon, K. D. 2000, PASP, 112, 537  
 Rodrigues, C. V., Magalhaes, A. M., Coyne, G. V., & Pirola, V. 1997, ApJ, 485, 618  
 Salpeter, E. E. 1955, ApJ, 121, 161  
 Savaglio, S., & Fall, S. M. 2004, ApJ, 614, 293  
 Schaerer, D. 2003, A&A, 397, 527  
 Schlegel, D. J., Finkbeiner, D. P., & Davis, M. 1998, ApJ, 500, 525  
 Schneider, R., Ferrara, A., & Salvaterra, R. 2004, MNRAS, 351, 1379  
 Shapley, A. E., Steidel, C. C., Adelberger, K. L., et al. 2001, ApJ, 562, 95  
 Shapley, A. E., Steidel, C. C., Pettini, M., & Adelberger, K. L. 2003, ApJ, 588, 65  
 Shapley, A. E., Erb, D. K., Pettini, M., Steidel, C. C., & Adelberger, K. L. 2004, ApJ, 612, 108  
 Simard, L., Koo, D. C., Faber, S. M., et al. 1999, ApJ, 519, 563  
 Steidel, C. C., Adelberger, K. L., Shapley, A. E., et al., 2003, ApJ, 592, 728  
 Steidel, C. C., Shapley, A. E., Pettini, M., et al. 2004, ApJ, 604, 534  
 Strickland, D. K., & Stevens, I. R. 2000, MNRAS, 314, 511  
 Todini, P., & Ferrara, A. 2001, MNRAS, 325, 726  
 Valencic, L. A., Clayton, G. C., & Gordon, K. D. 2004, ApJ, 616, 912  
 van Dokkum, P. G., Förster Schreiber, N. M., Franx, M., et al. 2003, ApJ, 587, L83  
 van Dokkum, P. G., Franx, M., Förster Schreiber, N. M., et al. 2004, ApJ, 611, 703  
 Vernet, J., Fosbury, R. A. E., Villar-Martín, M., et al. 2001, A&A, 366, 7  
 Vijh, U. P., Witt, A. N., & Gordon, K. D. 2003, ApJ, 587, 533  
 Walborn, N. R., Lennon, D. J., Haser, S. M., Kudritzki, R.-P., & Voels, S. A. 1995, PASP, 107, 104  
 Wang, J., Hall, P. B., Ge, J., Li, A., & Schneider, D. P. 2004, ApJ, 609, 589  
 Westerlund, B. E. 1997, The Magellanic Clouds (Cambridge University Press)  
 Whittet, D. C. B. 2003, Dust in the galactic environment, 2nd ed. (Bristol: Institute of Physics (IOP) Publishing)  
 Whittet, D. C. B., Shenoy, S. S., Clayton, G. C., & Gordon, K. D. 2004, ApJ, 602, 291  
 Witt, A. N., & Gordon, K. D. 1996, ApJ, 463, 681  
 Witt, A. N., & Gordon, K. D. 2000, ApJ, 528, 799 (WG00)  
 Witt, A. N., & Lillie, C. F. 1973, A&A, 25, 397  
 Zubko, V., Dwek, E., & Arendt, R. G. 2004, ApJS, 152, 211